Research Progress on Powder Injection Molding in Malaysia-A Review

Faiz Ahmad[1,*], M Rafi Raza[2], M Aslam[3], Ali Sameer Mohsin[1], Irfan Sherazi[2], Abqaat Naseer[1], Muhammad Ali[1], C.A. Shahed[1], A. Raza[1]

[1] Department of Mechanical Engineering Advanced and Functional Materials, Corrosion Research Center Universiti Teknologi PETRONAS, Perak, Malaysia.
[2] Mechanical Engineering Department, COMSATS University Islamabad, Sahiwal Campus, Pakistan
[3] Centre of Excellence in Science & Applied Technologies (CESAT) Islamabad Pakistan
Email: faizahmad@utp.edu.my

Received: 12-09-2022, Received in Revised form: 01-11-2022, Accepted: 01-11-2022, Published: 31-12-2022

Abstract

In this era, parts complexity, dimensional accuracy, and cost-effectiveness are one of the basic requirements of the modern industry. Most of the conventional manufacturing techniques have failed to fulfill the industry's needs. Powder injection molding (PIM) started in the early 70s, which is a combination of powder metallurgy and plastic injection molding that fulfills the gaps in conventional manufacturing techniques. In Malaysia, PIM was introduced by SIRIM Sdn Bhd Malaysia in late 2000. The latter few universities started working on PIM. Among all universities, the Advanced Functional Materials Research (AFM) group at Universiti Teknologi PETRONAS (UTP) started to work in 2008 under the direction of Prof. F. Ahmad and was decided to target various industries and their latest requirements. The work completed during the past 11 years has been published in various high-quality international journals, secure intellectual property (IP), i.e., trademarks, patents, a pre-commercialization grant from the government, one commercialization agreement, and signed a technology licensing agreement. They also worked on carbon Nanotube reinforced copper nanocomposite for thermal management and secured two patents. This project was commercialized for heat sink materials for LED Lights. The group is also working on controlling the orientation of fibers in the metal matrix to enhance thermal conductivity. Moreover, grafting graphene on metal oxide for its potential use as a radiation shielding material is one of the noble works. Currently, the group is working on the fabrication of soft magnetic material with enhanced permeability for potential use in hearing Aids, electric motors, and several other applications. Besides, bio-medical parts like a dental screw, bio-medical material of 316L SS reinforced by nano Titanium and additive manufacturing by using ultra-fused BASF 316L SS parts made through FDM represent the scope of works in PIM.

Keywords: PIM, Mechanical Properties, Microstructure, XRD, Corrosion Resistance

Introduction

Powder injection molding (PIM) was developed and patented in the 70s, however, was introduced in Malaysia in early 2000 via SIRIM Sdn Bhd Malaysia [1]. Later, University Kebangsaan Malaysia (UKM) initiated research activities on bio and nanocomposites using PIM. UiTM, Malaysia is also working on PIM for the development of porous metal implants [2]. PIM was started in Universiti Teknologi PETRONAS (UTP), in 2008 [3, 4]. The first project on PIM of 316L stainless steel (SS) was completed successfully in UTP and was managed to achieve a nanolayer of chromium oxide on the surface of the parts, which not only improved corrosion resistance but leaching of toxic metal ions was also minimized to a negligible level [5]. This project was continued and was decided to use micro-sized titanium and boron metal power with 316L SS to enhance densification, corrosion resistance, biocompatibility, and reduce the leaching of toxic metal ions. This study gathered very good data from in vitro trials and showed results that are very close to titanium. Clinical trials are still pending due to financial problems. Another project has been started by the same authors on biomaterials based on 316L SS and decided to use nano-size titanium as reinforcement [6]. In this study, the focus is to achieve greater densification, necessary surface modification, superior corrosion resistance, reduction of leaching of toxic metal ions, profound cell culture and their adhesion with the surface, and prediction of life of bio implant. In parallel, a noble work on the development of carbon nanotube (CNT) reinforced copper matrix composite for thermal management has been running. In this study, the CNT dispersion technique, method of producing feedstock, and material for the thermal management of electronics has been patented [7]. It would be worth mentioning here that during the past 20 years of PIM in Malaysia, the heat sink was contracted a technology license agreement for the product commercialization of heat sink for LED light application [8]. Another project based on a copper matrix reinforced with short carbon fiber has been running in which the aim is to control the orientation of short fiber in the flow direction to achieve a higher level of directional thermal conductivity. The project is on hold for further development and testing.

Table 1: List of IPs secured by prof. F Ahamd in powder metallurgy.

Product	Type	File/Grant No.
316L Stainless Steel for Orthopaedic Application	Trademarks	FY2011
Method Of Thermal Management of Portable Electronic Element Using Carbon Nanotube Metal Composite	Patent	PI2012000653
Metal Injection Molded 316L Stainless Steel for Bio and Dental Implants	Patent	PI2012700428
Hybrid Fiber Composite Drilling	Patent	PI2013001670
Process of Producing Nanocomposite Feedstock for Heat Dissipaters for Electronic System	Patent	PI2013001681
Biopolymer Composite and Processes for Making the Same	Patent	PI2016001521

Recently, two patents have been filed in favor of the author for the grafting of graphene and the method of producing feedstock and material for thermal management. related to the

https://doi.org/10.24949/njes.v15i2.720

field components using graphene was a very rare and new idea to produce engineering applications using graphene-reinforced materials. The technology of graphene grafting was applied to other materials such as iron oxide and successfully developed feedstock for both types of materials. Another aspect of this technology was an application in radiation shielding coating where grafted graphene with iron oxide can be used. The project is continuing and needs funding to translate this project into engineering applications of graphene. Presently, the development of soft magnetic material is ongoing, and have filed a patent to protect the process developed to achieve optimum grain size and permeability value of this material. The alloy is based on Fe-Ni and the process is optimized in terms of sintering parameters to achieve desired properties. This material can be applied in "Hearing Aid" to produce a low-cost device to make it affordable for people with such disabilities in developing countries, and further funding could take this area to move forward [9].

This is a summary of the development of PIM by these authors during the past ten years with minimum resources that have contributed to this technology for the benefit of industry and humans. The elaborated results that have been achieved will be discussed in the following sections.

Development of 316L Stainless Steel with improved Physical and Mechanical Properties

Introduction

Corrosion prevention of 316L SS is significantly important for biological and other industrial applications. In the human body, the existing corrosion causes allergic reactions and hypersensitivity that have serious consequences, i.e. hypersensitivity resulting in dermatitis, ulcers, and nervous system disturbance [10, 11]. The implants produced from wrought alloys need machining, heat treatments, and extra coating [12]. Therefore, residual stress appears during the machining process and carbide formations during the heat treatment process diminish the corrosion resistance of the implants. Currently, the parts produced through machining and casting need additional reinforcement of noble metals, carbides, or coatings to protect them from corrosion [13-24]. Moreover, chromium content is vital that creating a chromium oxide passivation layer to protect the SS in corrosive environments [25]. Based on the limitations of existing problems, an advanced fabrication technique is required to reduce the residual stresses and retain the maximum amount of chromium within the matrix and at the surface of the part. Presently, the biomedical parts products from various metal alloys need reinforcement, heat treatment, and additional coating on the parts to enhance their mechanical properties and corrosion resistance [14, 15, 26-29]. The advantage of the extant research work is that it produces material for medical applications with improved mechanical properties and corrosion resistance without any additional operation of such by using the Powder Injection Molding (PIM) technique.

PIM is the combination of powder metallurgy with plastic injection molding and is a rapidly growing technique that fulfills the gaps between other traditional metal fabrication techniques. It has the advantage of producing complex-shaped metal parts at a high production rate and low cost with superior dimensional accuracy and is equally applicable for both metals and ceramics [30, 31]. Powder injection molded parts have applications in aerospace, automotive, marine, medical, construction, electrical and electronics, jewelry, office equipment, recreation, and leisure goods [32]. The PIM market value size was USD 2.1 billion in 2015 and is projected to grow at a compound annual growth rate (CAGR) of 11.9% from 2014 to 2025. This is due to the intensification of the demands from end-use industries such as automotive and aerospace, consumer goods, and medical devices [33].

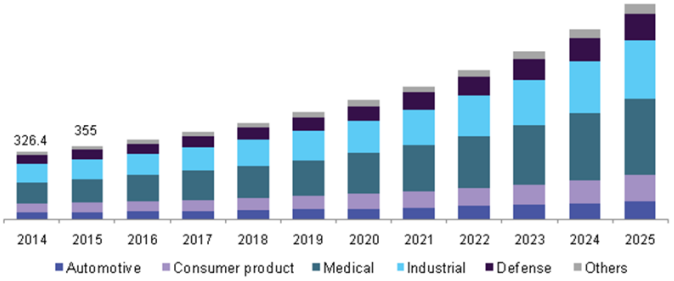

Figure 1: US Powder injection molding market 2014-2025 [33]

The PIM process consists of the four steps such as feedstock preparation, injection molding, debinding, and sintering [31, 34-36]. The processing steps involved in PIM are illustrated in Figure 2.

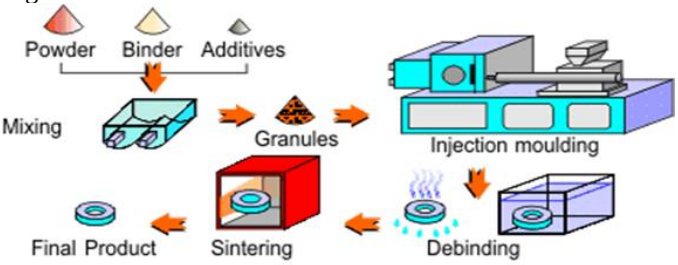

Figure 2: Powder injection molding process stages [37]

The success of the process and final mechanical properties depends upon several factors such as the metal powder shape, size, distribution, composition, particle reinforcement, binder system, powder mixing, molding, and the debinding parameters to achieve defect-free molded and sintered parts. The sintering parameters i.e. atmosphere, temperature, heating rate, dwell time and cooling rate affect the ultimate final density and mechanical properties [38-54]. Previous researchers discussed the effects of various processing parameters on the final properties of 316L SS [54-57]. Andrew Coleman et al, [54] used gas atomized 316L SS and investigated the effects of particle size distribution and sintering atmosphere on mechanical properties. Nattaya et al, [58] investigated the effects of different admixing and sintering atmospheres on the final product of 316L SS. The results showed that the nitrogen atmosphere was helpful to form nitride while the addition of a metal powder, PMTEC1 enhanced the grain growth and activated nitride eutectoid formation. Martin et al. [56] studied the effects of sintering parameters on mechanical properties of duplex SS and found that cooling rate is one of the significant factors that may affect the final properties. Raza et al. [48] explored the effects of the solid loading, and post-sintered cooling rate and concluded that the solid loading above the

critical solid loading reduced the mechanical properties and the higher post-sintered cooling rate is responsible to improve the mechanical and corrosion resistance properties.

Materials

In this study, water atomized 316L SS of D_{50} = 4.42 µm supplied by PACIFIC SOWA Japan was used. The chemical composition of the powder provided by the supplier is given in Table 2. The prepared 316L SS feedstock contained 65 vol % powder loading. The detailed procedure for molding and debinding is mentioned in our previous work [59]. The samples were sintered in a vacuum for 2 h at three different temperatures (1325˚C, 1360˚C, and 1380˚C) and post-sintered cooling rates (3˚C/min, 5˚C/min, and 10˚C/min) to study their effects on physical, mechanical and corrosion properties.

Table 2: Chemical Composition of water atomized 316L SS

Element	C	P	Si	Mn	Mo	S	Ni	Cr	Cu
Wt.%	0.02	0.03	0.36	0.07	2.1	0	10.5	16.6	0.1

Effects of cooling rate on shrinkage and densification

Cooling rates have a profound effect on the shrinkage of materials in terms of densification. A higher cooling rate decreased the cooling time which caused a reduction in grain size and porosity. The test samples sintered at higher temperatures, i.e., 1360˚C and 1380˚C the shrinkage was almost the same because higher sintering temperatures were mainly responsible for changing the morphology and location of the pores, which isolated them from the grain boundaries [60]. Figure 3 shows the effect of various cooling rates on densification. The results showed that a maximum sintered density of 96% was achieved at 1325˚C with a post-sintered cooling rate of 10˚C/min. It was observed that the sintered density was enhanced by increasing the post-sintering cooling rate due to the decrease in the solidification time that led to the reduced grain size, which increased the sintered density. The fast post-sintering cooling rate reduced the nucleation growth and resulted in the reduction in grain size improving the sintered density while increasing the sintering temperature mainly changed the morphology of the pores within the matrix [53]. From the results, it was concluded that given particle size achieved maximum sintered at a low sintering temperature (i.e. 1325˚C) which has a good agreement with the previous researchers [61]. The achieved sintered density was comparable with the ASTM standard for wrought stainless steel [62].

Effects of sintering parameter on tensile strength

Figure 4 shows the tensile strength value at different sintering temperatures and post-sintered cooling rates. The maximum tensile strength value of 501MPa with a good combination of elongation was achieved at 1325˚C with a cooling rate of 10˚C/min. Y Zhang et al. also measured the tensile strength of 560 MPa from the sintered parts of gas atomized 316L SS with a 58% elongation [63]. On the basis of the results, it is concluded that the relatively fast cooling rate is suitable to achieve an excellent combination of tensile strength and considerable ductility [64]. After achieving the maximum strength, the further increase in sintered temperature mostly changes the morphology of the pores within the matrix [43].

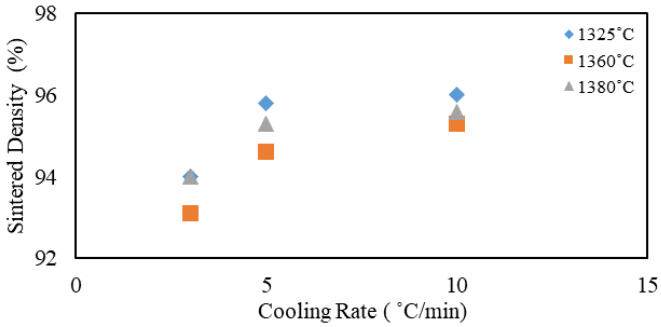

Figure 3: Sintered density vs. cooling rate at different temperatures

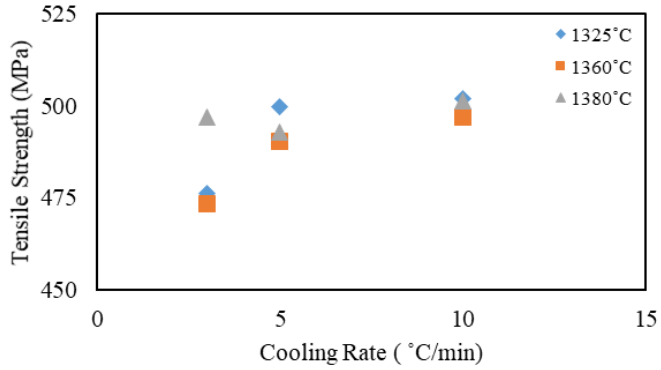

Figure 4: Effects of post-sintering cooling on tensile strength of 316L SS

Effects of cooling rate on Microstructure

The typical microstructures of the 316L SS are shown in Figures 5 and 6 for the sintered samples at 1325˚C. The pores were irregular in shape and distributed across the grain boundaries as well as within the matrix. The SEM results show that at all temperatures with a cooling rate of 10°C/min, there was less porosity as compared to those with a cooling rate of 5ºC/min. At this temperature, the pores were irregular in shape. The grains were well grown during the cooling rate of 10ºC/min, which reduced the porosity [44]. The difference in the grain growth and the reduction in porosity is clear in Figures 5 and 6.

The XRD results showed that there was no carbide phase detected with a post-sintering cooling rate of 10˚C/min as is shown in Figure 7. The structure was FCC austenitic. It was found that the carbon content was reduced from 0.00636 % to 0.00374 %, which was present in the form of traces and the higher post-sintering cooling rate provided insufficient time for carbide formation

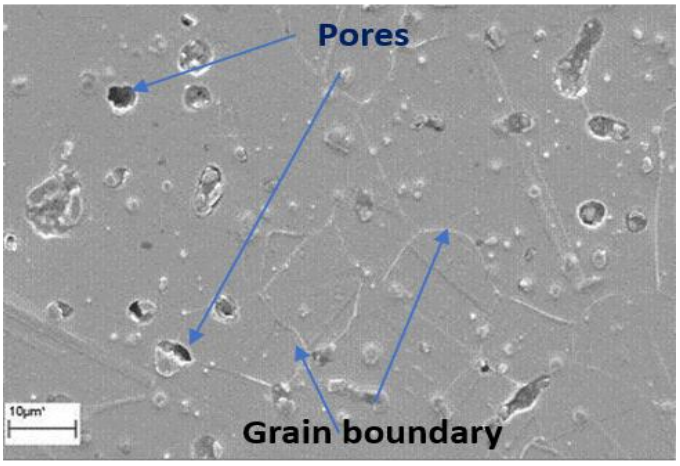

Figure 5: SEM image of sample sintered at 1325˚C with a cooling rate of 5˚C/min

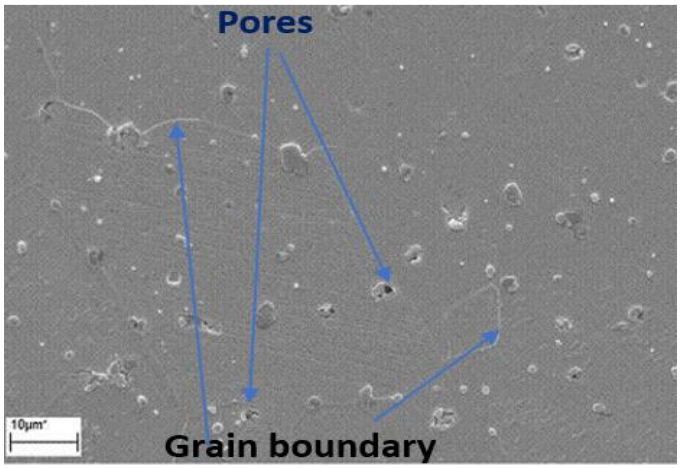

Figure 6: SEM micrograph of sample sintered at 1325˚C with a cooling rate of 10˚C/min

.

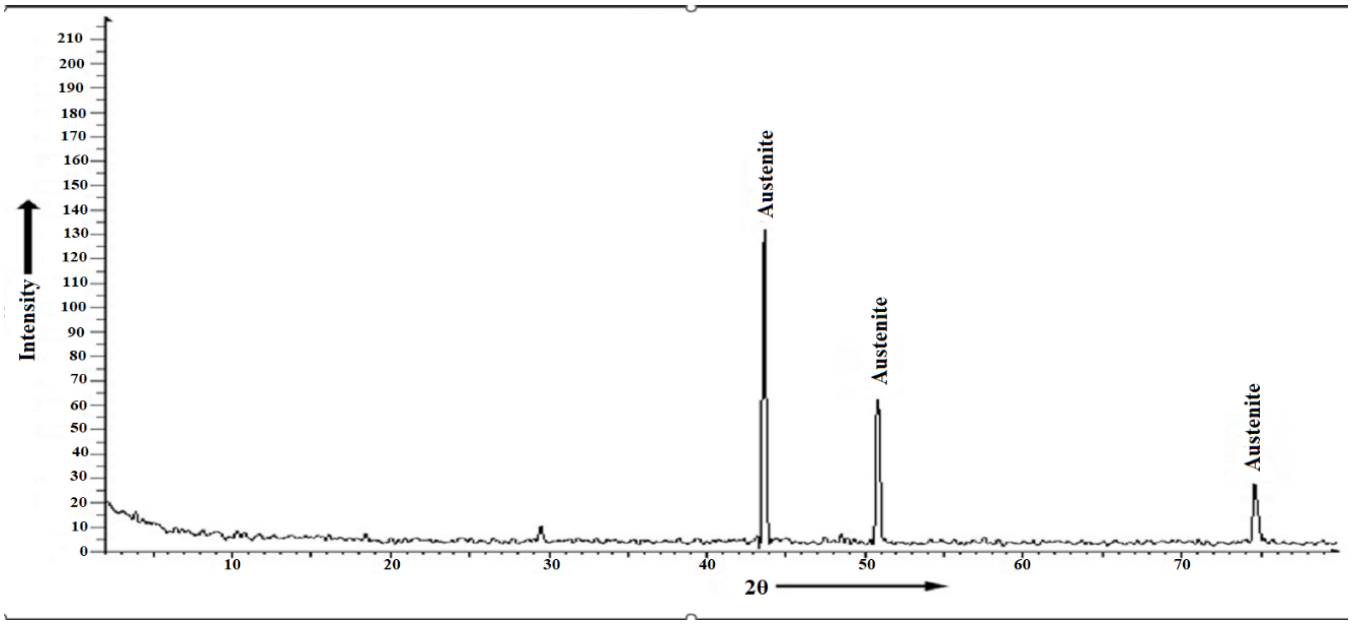

Figure 7: XRD pattern showing an austenitic structure in vacuum sintered 316L SS

As the sintering temperature was increased, the particles moved closer to each other, reduced the number of pores, and changed their morphology. Some significant micrographs of the sintered samples at 1380˚C were taken using FESEM. The micrograph shown in Figure 8 revealed that increasing the sintering temperature influenced the shape of the pores. The pores became finer, round, and isolated as compared to sintering at a lower temperature of 1325˚C.

Effects of Cooling rate on Corrosion rate

The corrosion rate was measured after immersion of test samples in Ringer's solution for 30 days. The weight loss measurement was performed according to ASTM G-01 and ASTM F746-87. The relationship between the corrosion rate, sintering temperature, and post-sintering cooling rate is provided in Table 3.

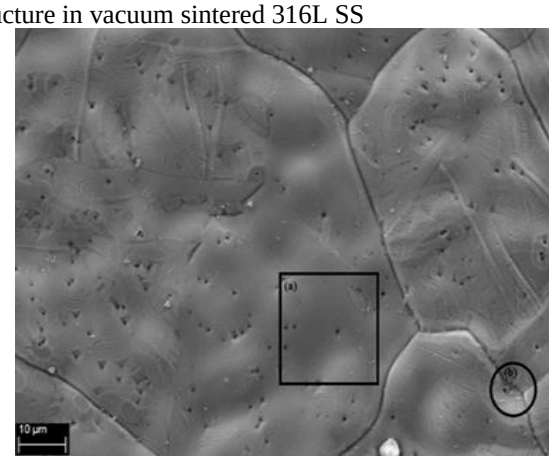

Figure 8: FESEM image of sample sintered at 1380˚C with a cooling rate of 10˚C/min

Table 3: Effects of vacuum sintering and post sintering cooling rate on corrosion rate

Corrosion rate (mpy)								
1325˚C			1360˚C			1380˚C		
3˚C/ min	5˚C/min	10˚C/ min	3˚C/ min	5˚C/ min	10˚C/ min	3˚C/ min	5˚C/ min	10˚C/ min
0.39	0.25	0.17	0.27	0.42	0.12	0.38	0.42	0.22

Based on the results, it was concluded that the corrosion rate decreased by increasing the post-sintering cooling rate. The improved corrosion resistance would be achieved using high vacuum sintering, which might be helpful to minimize the evaporation of Cr during sintering. This was followed by a higher post-sintering cooling rate that would provide less diffusion time to the chromium within the matrix and shorten the time for the carbide formation [10, 65-68]. This resulted in the existence of Cr at the surface of the test sample in the form of a passive oxide layer (Cr_3O_2) that improved the corrosion resistance. Johnson *et al.* [69] tested the corrosion rate of 316L SS in basic and acidic environments and found that the corrosion rate varied from 0.88 mpy to 36 mpy, respectively. The achieved results were better than the reported results tested in a chloride environment [70].

Analysis of the toxic metal ions in vacuum sintered samples

In the chloride environment, the stainless steel was immersed for 30 days to measure the release of Fe, Ni, and Cr ions. The Ni and Cr ions cause allergic and carcinogenic reactions within the human body [71]. Table 4 shows the overall results of Fe, Ni, and Cr ions released from test samples.

Table 4: Release of metal ions from sintered samples in Ringer's solution

Formulation	3˚C/min			5˚C/min			10˚C/min		
	Ni	Cr	Fe	Ni	Cr	Fe	Ni	Cr	Fe
65% SL	0.0006	0.0002	0.0008	0.0004	0.0001	0.0004	0.0001	0.0006	0.0036

* Ppm unit for metal ions

The results of the metal ions also showed that by increasing the post-sintered cooling rate, the release of the metal ions was reduced. This was considered due to the vaporization of Cr atoms being slow in the vacuum and the post-sintering cooling cycle. The diffusion of Cr is slow as compared to the other metals, i.e., Fe and Ni, so at higher cooling rates, most of the Cr is retained at the surface of the part and formed the passive oxide layer. This passive oxide layer protected the parts against the chloride environment. Secondly, the fast cooling minimized the possibility of chromium and carbon reaction for carbide formation. The passive oxide layer acted as a barrier to reduce the release of metallic ions. Previous studies have shown that 0.1 ppm is the critical value for Ni and 30 ppm is the limit where it becomes cytotoxic to response [72, 73]. In this study, the number of metal ions released during the testing was much lower than the present in the human body [74-77].

Conclusions

The results of injection-molded vacuum sintered samples showed that sintering parameters have significant effects on the mechanical, microstructure, and corrosion resistance properties. The results also showed that the sintering temperature of 1325ºC with a post-sintered cooling rate of 10ºC/min is the most appropriate sintering temperature and cooling rate to achieve optimum physical and mechanical properties. The shrinkage is within the range required for PIM. The maximum sintered density and tensile strengths were 96% and 501MPa with optimized sintered parameters. The microstructure of sintered test samples showed that porosity was decreased by increasing the post-sintered cooling rate and by increasing the sintering temperature the pores become round, isolated, and distributed within the matrix. Corrosion data measured by the weight loss method showed that the minimum corrosion rate was 0.17 mpy with minimal leaching of metal ions.

Development of Modified 316L SS for Dental Implant Application

Introduction

The powder injection molding technique can produce defect-free intricate shape parts with minimal secondary operations. Four main 316L SS formulations were designed. The first two formulations include admixed titanium and elemental boron (0.5, 1, and 1.5 wt. %) with powder water atomized stainless steel powder. The third formulation was prepared by using a 316L SS bimodal mixture of spherical and irregular particles of different sizes. The fourth formulation was designed by preparing a series of formulations with a solid loading of powder gas atomized between 63 to 72 vol %. The samples were sintered in a vacuum (10^{-6} torr) at four different temperatures. Two-stage sintering followed by the post-sintering cooling rate of 20ºC/min. The powder injection molding process is shown in Figure 9. The results showed that the addition of boron and titanium enhanced the sintered density by 98.5% and 95% respectively. The current density and corrosion rate were observed at 0.188 μA/cm^2 and 0.081 mpy for titanium admixed samples and it is close to commercially pure titanium current density of 0.12 μA/cm^2 and corrosion rate of 0.026 mpy. Cytotoxicity results showed that the cell viability of titanium admixed formulation is 85% of commercially pure standard titanium. It was observed that the tensile strength of titanium-containing samples exhibited 484 MPa along with 37% fracture elongation. Optimal sintering parameters helped to develop a nano-size passive layer of Cr_2O_3 on the surface confirmed by x-ray photoelectron spectroscopy results. This passive layer minimized the leaching of Chromium and Nickel

toxic metal ions to values of 0.0021 and 0.0005 ppm respectively, and this is far below the critical value for the human body. Test samples results show that the new material developed in this study exhibits biocompatibility and is comparable to titanium standard in functional properties. This material is expected to provide a low-cost solution to dental implants for patients and significant impact on the economy.

To explore alternative cost-effective manufacturing methods for producing implants, PIM technology was evaluated. This technique is regarded as a very promising net shaping for intricate parts, due to its advantages for complex geometry, precision, and series production of implants with high performance, without secondary operations [78-80]. However, there are a number of issues associated with the PIM process like non-homogeneous feedstock, powder binder separation [81], poor green strength, and evaporation of chromium from the outer surface during the sintering process. [59, 82]. Therefore, to solve the above-mentioned problems, highly densified biocompatible 316L SS implants containing a composite nano passive layer of iron and chromium oxide are required. To enhance the densification by addition of nano elemental boron (nB) and micron size titanium (Ti), and linkage of densification with biocompatibility and cytotoxicity of powder water atomized (PWA), powder gas atomized (PGA) and bimodal packing approach (P25/75) have not been investigated. Based on the research problem this study was designed to develop 316L SS with enhanced densification, good corrosion resistance, high mechanical strength (tensile strength and hardness) and biocompatibility through:

- Investigating the influence of shape and size of 316L SS powder material.
- Evaluating the effects of bimodal packing approach of 316L SS powders.
- Analyzing the effects of admixed nano-size elemental boron and titanium with 316L SS powders.
- To identify the optimal sintering parameters at which the diffusion of Chromium would be enormous to make available the essential flux of chromium to the outer surface to support the formation of chromium oxide passive thin film and lower the leaching of toxic metallic ions in the physiological environment.

Methodology

The flow diagram of the research activities of this study is shown in Figure 9 and feedstock formulations in Figure 10.

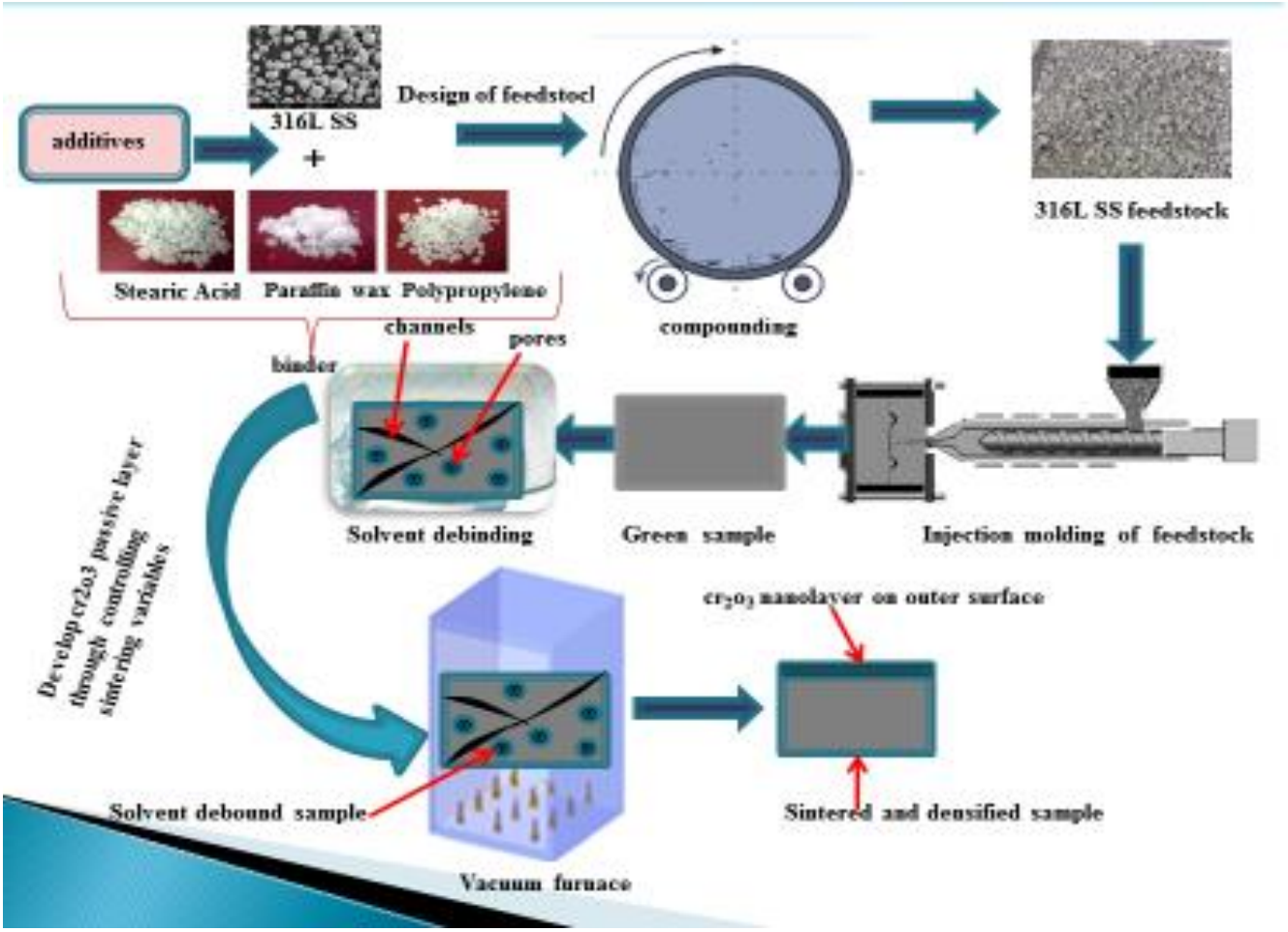

Figure 9: The flow diagram of research activities

.

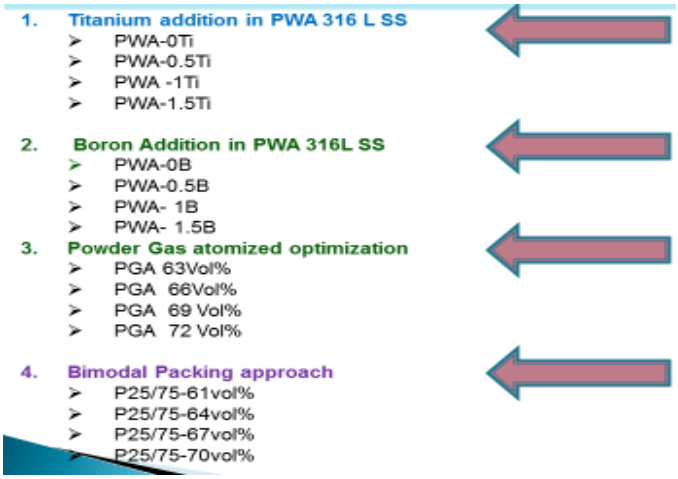

Figure 10: Feedstock formulations

The sintering cycle with controlled cooling is shown in Figure 11. The digital image of sintered parts is shown in Figures 12 and 13.

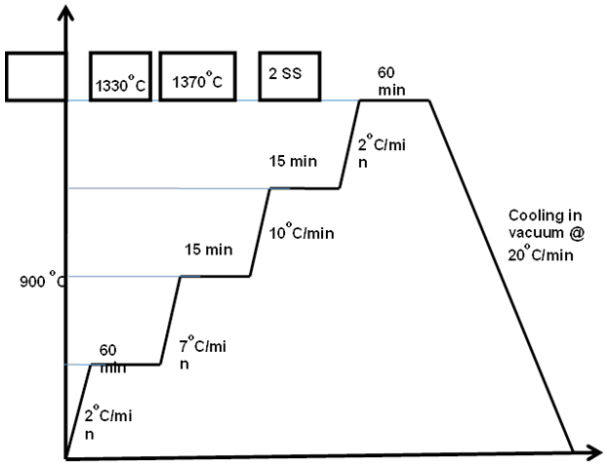

Figure 11: The sintering cycle with controlled cooling

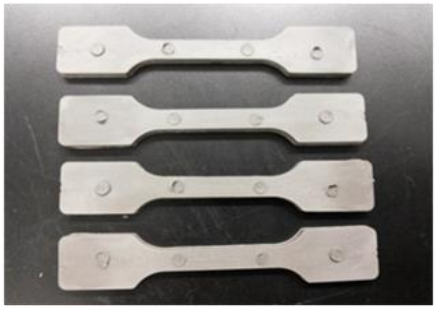

Figure 12: Digital image of sintered samples

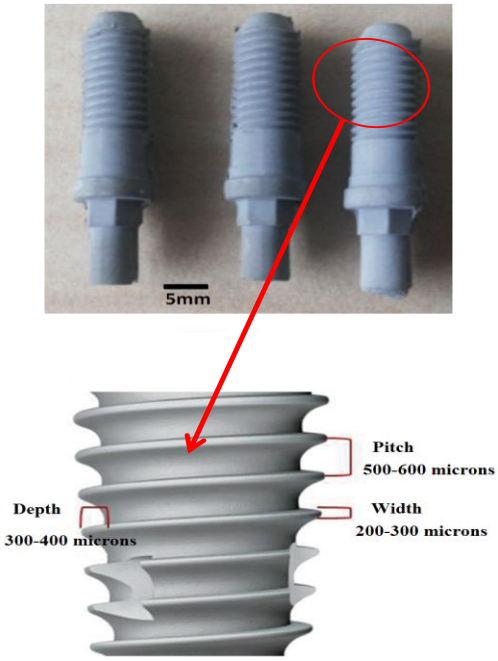

Figure 13: Digital image of sintered dental implant

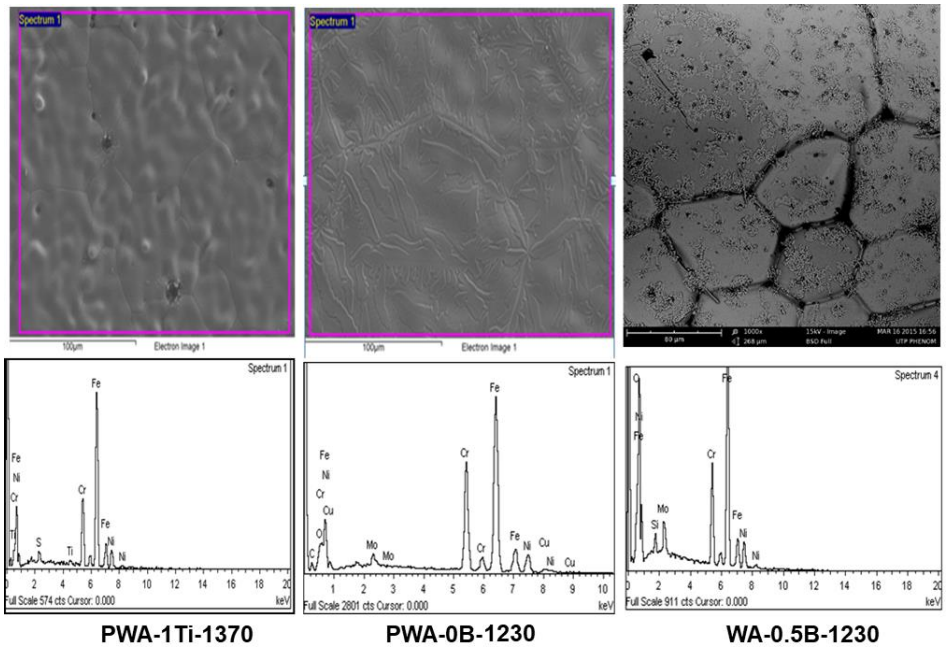

Figure 14: EDX of the outer surface of sintered materials.

The FESEM images of PGA sintered parts are shown in Figure 15.

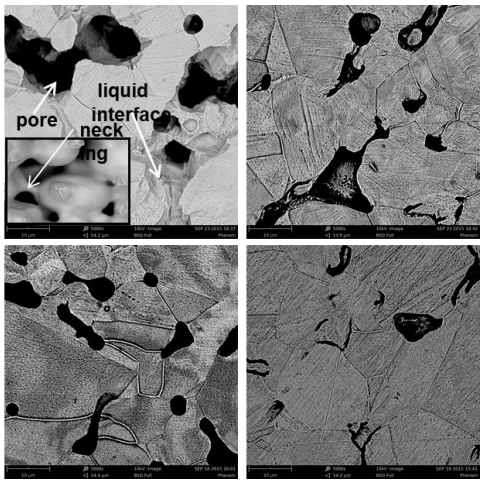

Figure 15: Microstructural analysis of PGA sintered parts.

Mechanical Properties of materials sintered at various temperatures are given in Table 5 and the microstructure of fractured surfaces is shown in Figure 16.

Table 5: Tensile strength of materials sintered at various temperatures

Formulations	1230°C	1330°C	1370°C	2SS
PWA-0B	425	434	446	424
PWA-0.5B	415	401	390	411
PWA-0TI	421	441	452	426
PWA-1Ti	422	440	484	454
P25/75-61	406	432	448	429
P25/75-67	432	445	466	445
PGA-63	280	333	364	351
PGA-69	295	356	382	360

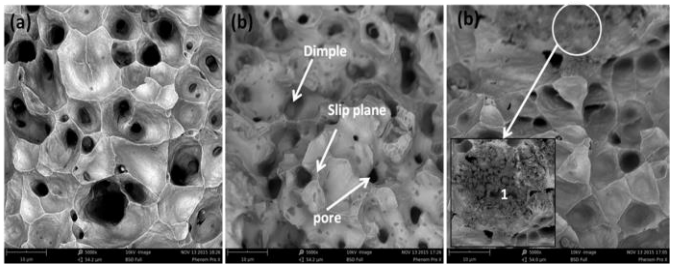

Figure 16: SEM microstructure analysis of tensile fracture.

The corrosion rate of sintered parts is given in Table 6. The corrosion resistance analysis is described in Figure 17 and data is given in Table 7. The Cytotoxicity Assessment is shown in Figure 18.

Table 6: Corrosion rate of sintered Materials

Formulations	Corrosion rate (mpy)	
	1230°C	1370°C
PWA-0B	0.527	0.336
PWA-0.5B	0.808	0.905
PWA-0Ti	0.527	0.336
PWA-1Ti	0.118	0.081
P25/75-61	2.055	1.614
P25/75-67	0.532	0.312
PGA-63	3.798	3.533
PGA-69	3.757	2.713

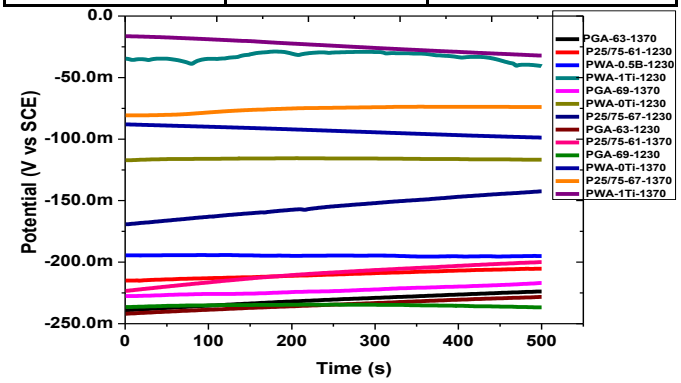

Figure 17: Corrosion resistance analysis

Table 7: Corrosion resistance analysis

samples	I_{Corr} (μA/cm^2)
PWA-1Ti-1370	0.18
PGA-69-1370	6.24
CP Ti	0.12

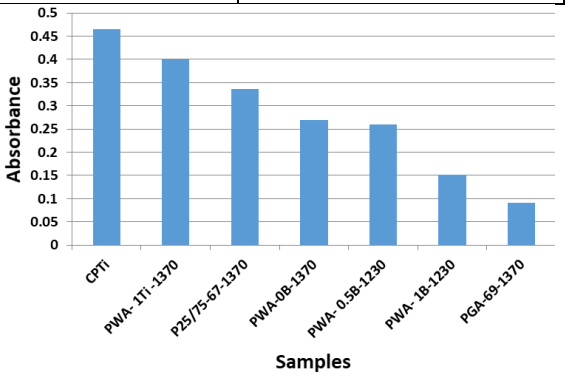

Figure 18: Cytotoxicity Assessment

Fibroblast cells were isolated from gingiva tissues and cultured in Dulbecco modified eagle medium (DMEM) and the medium was changed after 48h. After seeding the data was recorded using a microplate reader as shown in Figure 19. Only PGA-69-1370 shows comparatively less cell viability than control group. The XPS analysis is shown in Figure 20. A passivation layer of Cr_2O_3, Fe_2O_3 formed in the matrix that negate the corrosion. Also, Ni_2P is famous for oxygen evolution and therefore formation of oxide passivation layer was accelerated [83].

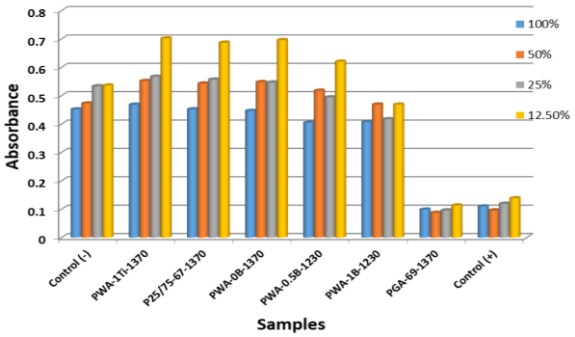

Figure 19: Cytotoxicity Assessment.

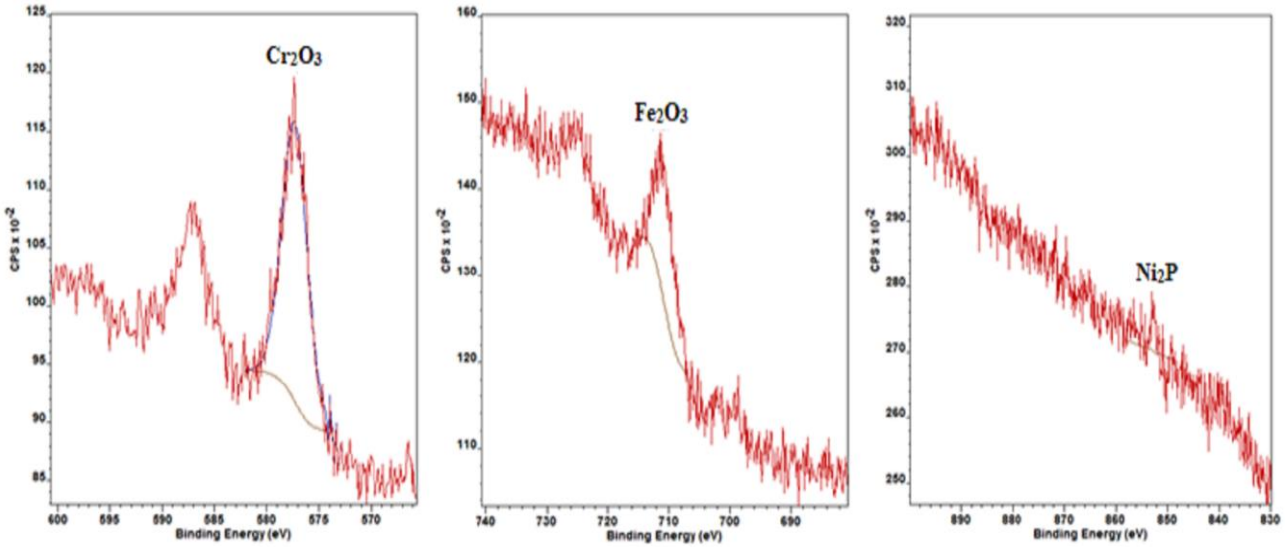

Figure 20: XPS Analysis

Leaching of Toxic Ions

The standard and experimental values of toxic ions are given in Tables 8 and 9, respectively. The elemental concentration is shown in Figure 21.

Table 8: Standard Values

Toxic ions	Standard value
Fe	0.176
Cr	0.1119
Ni	0.0022

Table 9: Experimental value

Formulations	Elements concentration (ppm)		
	Fe	Cr	Ni
PWA-0.5B-1230	0.0042	0.0039	0.0002
PWA-1Ti-1370	0.0036	0.0021	0.0005
PGA-69-1370	0.8847	0.5588	0.3832
P25/75-67-1370	0.0009	0.0001	0.0133

Future direction of PIM of 316 LSS

Recently a work based on reinforcing nano titanium in 316L SS powder has been working to study its effect on densification, surface roughness, cell culture, and adhesion with sintered parts to assess the life of the implant.

Short Carbon fiber reinforced copper matrix composites

This study aimed to develop short carbon fiber reinforced copper matrix composites via PIM. Several types of feedstocks were prepared, and injection molded to produce green parts and sintered. Fiber orientation was controlled by controlling the flow pattern. The geometry of the mold was designed to achieve convergent flow and this design resulted in highly aligned short fibers in the molded and sintered composites. The orientation of fibers was 22°. Following mold, geometry was used as shown in Figure 23. Fiber orientation angles and FESEM micrograph is shown in Figure 24. Short carbon fiber orientation in sintered copper composites is shown in Figure 25.

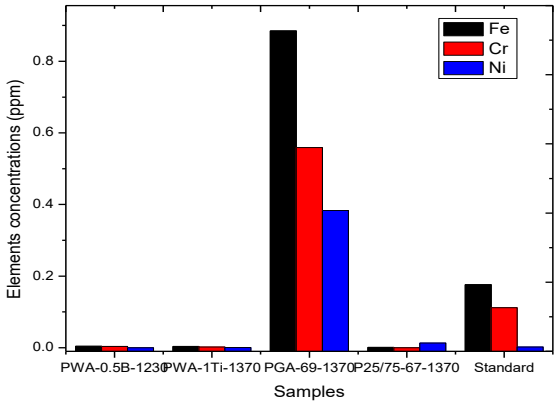

Figure 21: Elemental concentration

The digital images of green and sintered dental implants are shown in Figure 22.

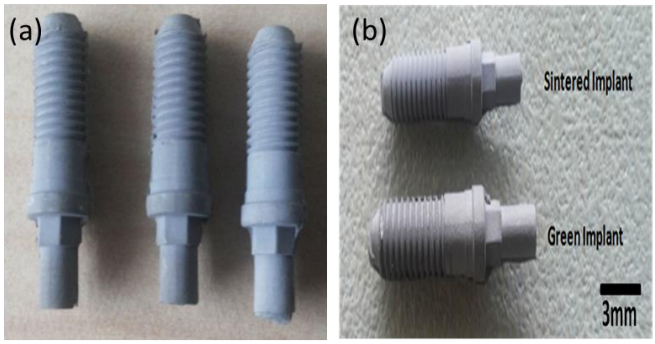

Figure 22: Digital image of (a) Green dental implant and (b) Sintered dental implant

Figure 23: Mold geometry

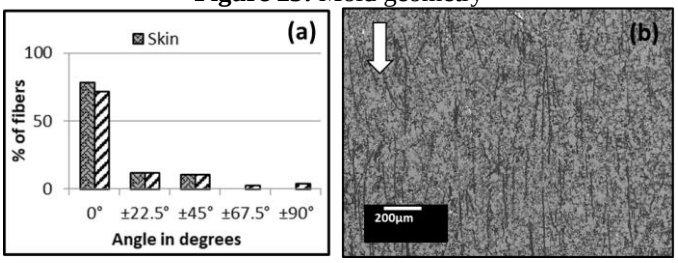

Figure 24: (a) Fiber orientation angles versus percentage for Section B Cu-10%CF and (b) FESEM micrograph showing fibers in flow direction at Section B: Core for Cu-10%CF.

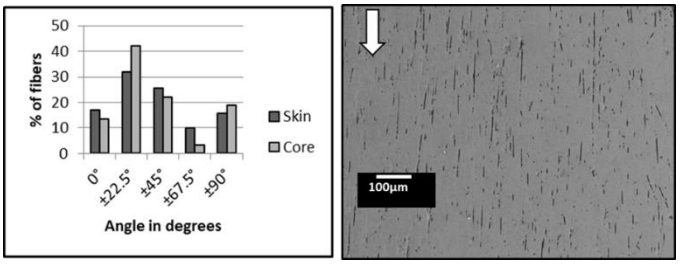

Figure 25: Short carbon fiber orientation in sintered copper composites

This project has great potential but funding problems to move forward.

Development of Carbon Nanotubes Reinforced Copper Matrix Nanocomposites via Powder Injection Molding

Introduction

The next generation of high-performance electronic devices requires materials with special thermal properties such as high thermal conductivity and low coefficient of thermal expansion. Carbon nanotubes (CNTs) reinforced Cu matrix nanocomposite hold the promise of delivering high-performance heat sink material. This research aims to develop high thermal conductive material of multiwalled carbon nanotubes (MWCNTs) reinforced Cu matrix nanocomposites by means of a combined technique of nanoscale dispersion (NSD) followed by the PIM process. Commercial Cu powder and purified MWCNTs were used as a solid loading and mixed with a polymer binder system to prepare the feedstock for the PIM process as shown in Figures 26 and 27. After the injection molding step, solvent and thermal debinding processes were carried out to remove the binder. The samples were sintered at 1050°C for different dwell times in an argon atmosphere. Prepared samples were then examined using various characterization techniques and the results showed that after using NSD, the wettability between Cu and individual MWCNT was increased and MWCNTs dispersion inside the Cu matrix was significantly improved. Thermal conductivities of Cu/MWCNTs nanocomposite with 10 vol.% MWCNTs sintered at 1050°C for 150 min showed the highest increase in thermal conductivity with an increase of 76% (581 W/m. K) compared to that of unreinforced sintered pure Cu (330 W/m. K). The coefficient of thermal expansion (CTE) of Cu/10 vol.% MWCNTs nanocomposites were reduced by 33% compared to that of pure sintered Cu. The modulus of elasticity of Cu/10 vol% MWCNTs nanocomposite was increased by 48% (124 GPa) compared to pure sintered Cu (84 GPa).

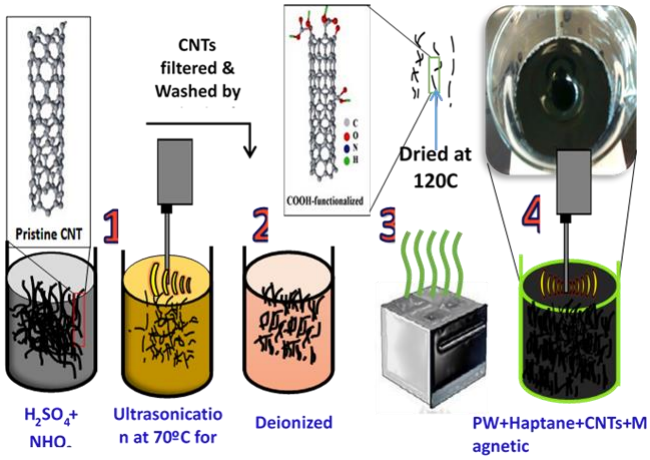

Figure 176: Materials and Preparation of Test Samples

Figure 27: CNT cake developed for feedstock

The preparation of feedstock is shown in Figure 28. The digital images of heat sinks are shown in Figure 29.

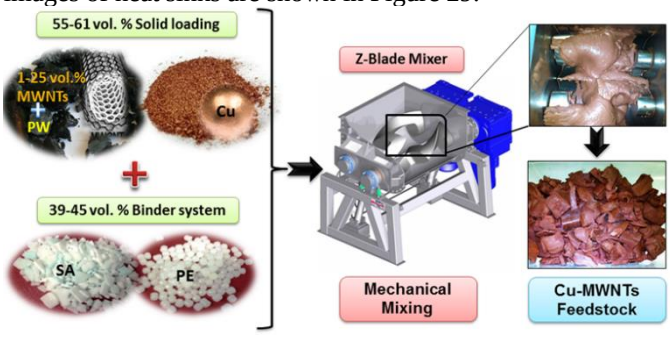

Figure 28: Mixing and preparation of MWCNTs-Cu-binder feedstock

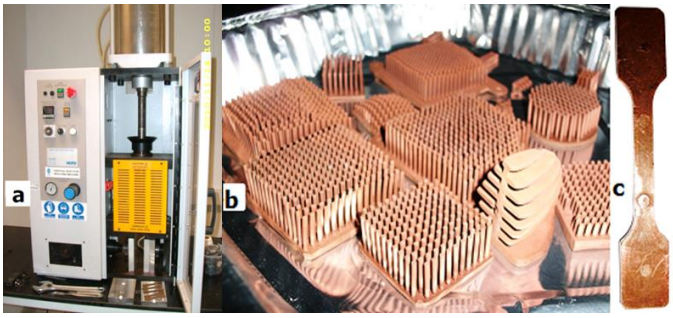

Figure 29: VIM machine (MCP-100KSA) was used to produce green samples of Cu/MWCNTs, (b) heat sink molded samples, and (c) dog bone molded samples.

Solvent debinding was based on binder-solvent interdiffusion; the temperature and time were varied to obtain the optimum debinding parameter. Three temperatures were examined (60ºC, 65ºC, and 70ºC) and the samples were held for different dwell times (1-7 h). The thermal debinding process burnt the remaining binder after the solvent extraction. To determine the optimum thermal cycle, thermal gravimetric analysis (TGA) was performed. The thermal debinding and sintering process were carried out at the same time using a box furnace. The samples were sintered at 950°C, 1000°C, and 1050°C. The effects of sintering temperature and the sintering dwell time on the final properties of the metal injection molded Cu/MWCNTs were investigated. The last stage was initiated from 500°C to three different sintering temperatures (950, 1000, and 1050°C) and three different dwell times (60, 90, and 120 min) at a heating rate of 5°C/min. The variation in sintering parameters was carried out to determine the optimum conditions for producing high-performance heat sink material. Figure 30 demonstrates a schematic of the individual steps involved in this method.

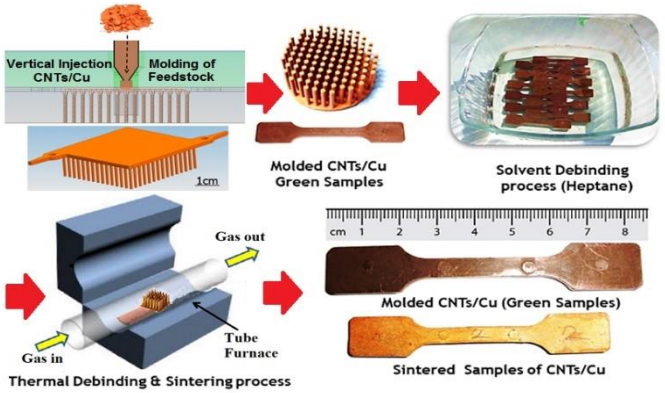

Figure 30: Fabrication stages of Cu- MWCNTs nanocomposites

Thermal Conductivity

Sintered parts were tested for physical, mechanical, and thermal properties of the nanocomposites. However, in this work, thermal properties have been highlighted of the developed material. Thermal conductivities were measured using a NETZSCH model LFA 447 NanoFlash™ apparatus (LFA447, Netzsch, Germany) as shown in Figure 31. The NanoFlash works with the flash method according to international standards ASTM E-1461, DIM EN 821, and DIN 30905. Specimens were cut into a round shape and polished using fine sandpaper. The specimens' dimensions were 12.7 mm in diameter and 2 mm in thickness. To obtain accurate results, three specimens for each formulation was assessed and five reads for each specimen were measured and finally, the average value was recorded. The temperature rise on the back face of the sample is measured using an In-Sb detector.

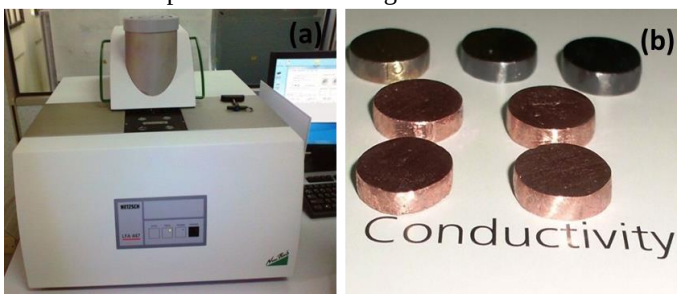

Figure 31: (a) NanoFlash machine, (b) samples for thermal conductivity measurement

The comparison between experimentally measured thermal conductivities and theoretical prediction models is shown in Figure 32.

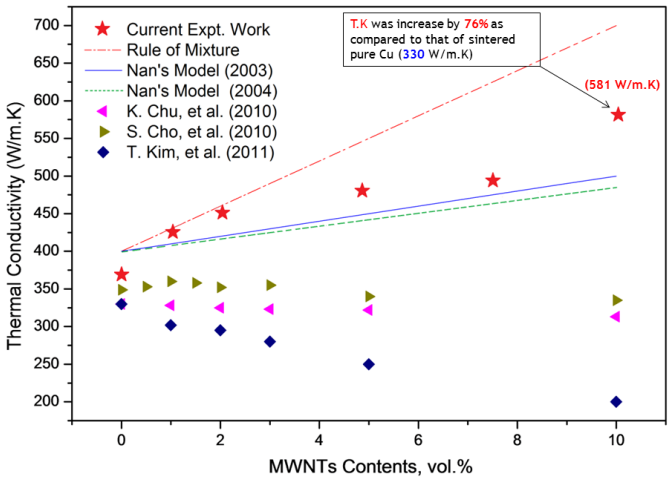

Figure 32: Comparison between experimentally measured thermal conductivities of sintered Cu/MWCNTs nanocomposites sintered at 1050 °C for 2.5 h, and rule of mixture, theoretical prediction models [84, 85], and the previous exp. works reported by Cho *et al.*, Chu *et al.*, and Kim *et al.*, [86-88].

FESEM micrograph of Cu/10 vol.% MWCNTs showing dispersion are shown in Figure 33. High-resolution TEM micrograph of Cu/10vol.% MWCNTs nanocomposite revealing high-quality MWCNTs bonded and implanted into the Cu particle is shown in Figure 34.

Hardness

The hardness of the sintered Cu/MWCNTs samples was measured according to the ASTM E18-11. Three samples from each formulation were assessed and five reads for each sample were measured, and finally, the average value was recorded. Figure 35 shows the results of the hardness test along with the relative density values of Cu/MWCNTs nanocomposites at different contents of MWCNTs. It can be clearly seen that after adding 1 vol.% MWCNTs the hardness value was increased significantly by 118% (120 Hv) compared to that of the unreinforced Cu matrix (55 Hv) as shown in Figure 35.

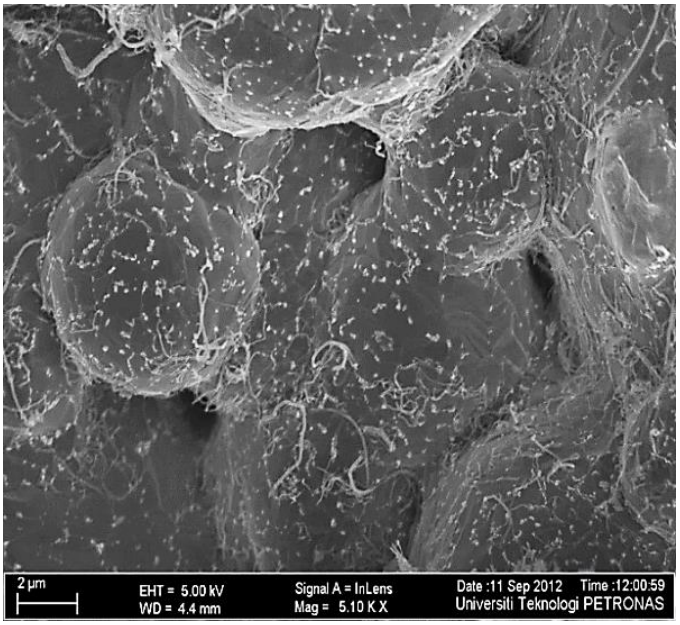

Figure 33: FESEM micrograph of Cu/10 vol.% MWCNTs showing dispersion on CNTs

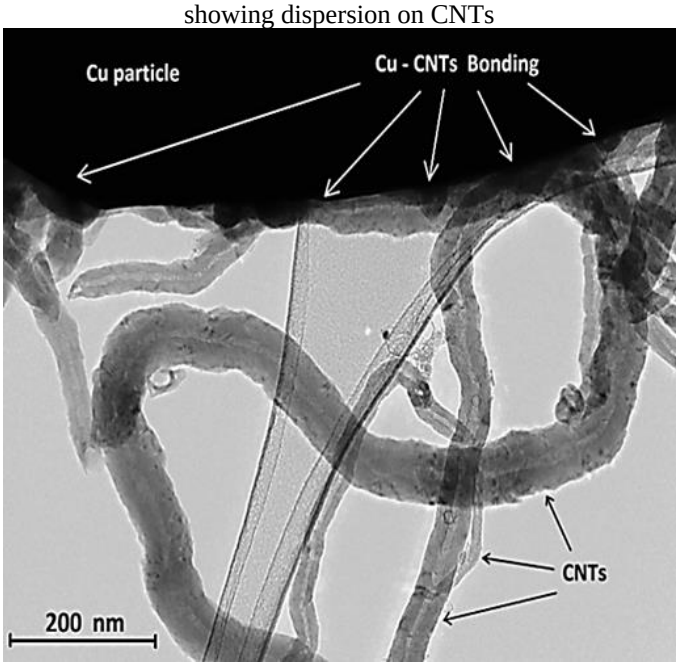

Figure 34: High-resolution TEM micrograph of Cu/10vol.% MWCNTs nanocomposite revealing high-quality MWCNTs bonded and implanted into the Cu particle

By increasing the MWCNTs contents up to 10 vol.%, the hardness value was slightly decreased to 94. Non-uniform dispersion and MWCNT agglomeration were responsible for hardness decreasing. According to Twinkle et al. [89], the non-uniform carbon nano-tube distribution reduced the stiffness of the material, therefore the buckling and hardness of the metal were also reduced. Although, these values are much higher than that of the unreinforced Cu matrix.

Young's Modulus

To understand the influence of adding different amounts of MWCNTs to the Cu matrix on the mechanical properties, a comparison between the experimental results, theoretical prediction models, and previews of published data on similar nanocomposites were presented. Several micromechanical models have been developed to predict the enhancement of stiffness due to the presence of fiber in a matrix. These models consider the volume fraction, stiffness, distribution, and orientation of the fibers in the matrix. For example, the rule of mixtures (ROM) assumes that the fibers are parallel, continuous, and run throughout the length of the sample.

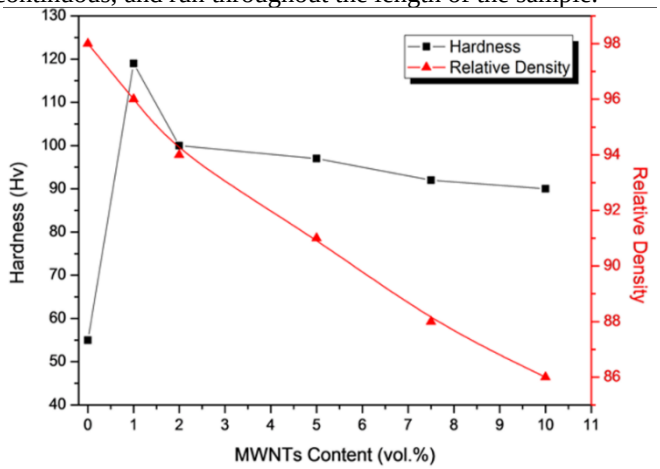

Figure 35: Hardness measurement and relative density of Cu/MWCNTs nanocomposites

When the load is applied parallel to the length of the fibers, it is known as a Voigt condition. Assuming the iso-strain condition, the load is distributed among the fibers and the matrix, and the composite elastic modulus is represented by $E_{\|}$ (also known as ROM), as shown in equation 1 [90]:

$$E_{\|} = V_f E_f + (1-V_f)E_m \quad (1)$$

When the load is applied normally to the length of the fibers, it is known as the Reuss condition. The total strain is distributed among the fibers and the matrix in such a manner that the load is the same in both, and the composite elastic modulus is represented by $E_{\perp}$, as shown in equation 2 [90]:

$$E_{\perp} = E_f E_m / [E_f (1-V_f) + E_m V_f] \quad (2)$$

However, in actual composites, the CNTs are distributed randomly and in such a case, the resultant elastic modulus is a weighted average of both parallel and perpendicular types of loading geometries. The elastic modulus for the randomly oriented CNT composites can be given by the combined Voigt-Reuss Model (*modified* ROM), which is given as follows [91]:

$$E_{\|} = 3/8\, E_{\|} + 5/8\, E_{\perp} \quad (3)$$

The modulus of elasticity (Young's modulus) of Cu/MWCNTs nanocomposites sintered at 1050 °C for 2.5 h was increased with the addition of MWCNTs. A 7.5 vol% MWCNTs-reinforced Cu matrix nanocomposites showed the highest young's modulus of 127 GPa, which is 52% higher than that of the Cu matrix (84 GPa), which was fabricated by the same process without adding MWCNTs. The same composite showed a strong agreement with the previously published work by Seung *et al.* [92] (they used a molecular level mixing technique to fabricate the Cu/CNTs samples) and below the value predicted using the ROM model. This is mainly because the ROM model does not take porosity shape into account and assumes that the reinforcement is continuous. In the case of 10 vol.% MWCNTs-reinforced Cu, Young's modulus was 124 GPa, which corresponds to an increase of 48% compared to that

of the unreinforced Cu matrix, as shown in Figure 36. This is due to the load sharing between the Cu matrix and MWCNTs. Individual MWCNTs can withstand higher loads than the copper matrix and hence there is a substantial increase in the mechanical properties of Cu/MWCNTs nanocomposites.

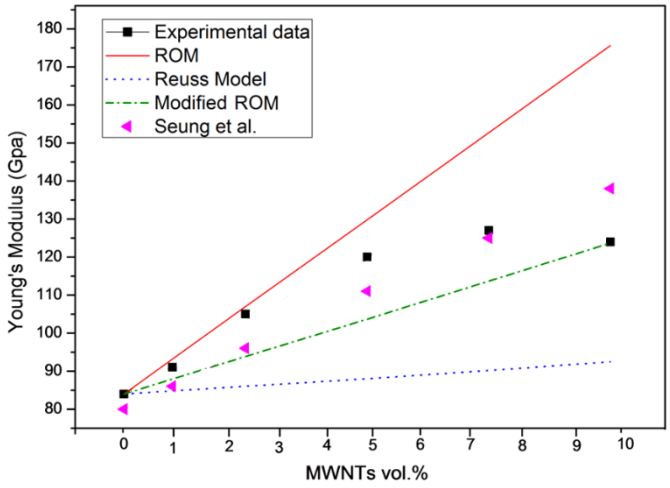

Figure 36: Young's modulus comparison between current experimental results, theoretical models, and data of preview work [92]

Grafting of Metallic Oxides on Graphene Nanoplatelets for Development of Reinforced Copper Composites via Powder Injection Molding

This is a very novel idea to translate graphene into engineering applications and produce components via PIM. As dispersion of nanoparticles in matrix materials is always a great challenge, specially CNTs and graphene. The grafting of graphene is in progress with various particles, however, the grafting of graphene nanoplatelets with metal oxide for the preparation of feedstock and injection molding is not reported anywhere yet. In this study, several types of graphene were used and were finally able to select purchased from Sigma Aldrich, USA. The digital images of sintered heat sinks are shown in Figure 37.

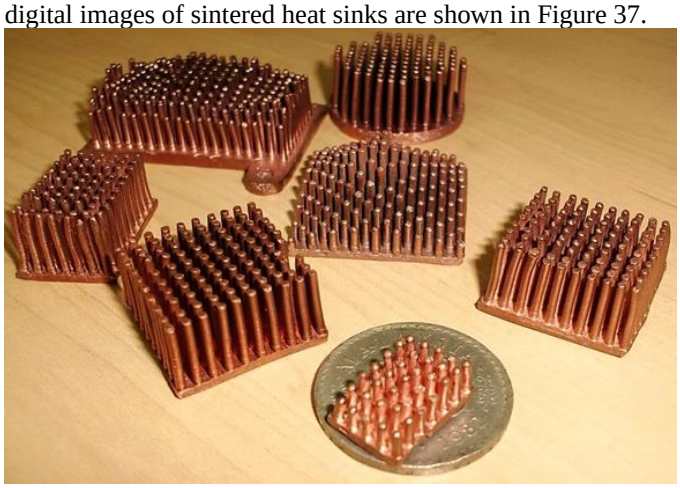

Figure 37: Shapes of Heat Sink Molded and Sintered

Also, it is determined that GNP has a minimum level of defects that will not affect the properties of the composite. For dispersion, the ratio of the solvent mixture was also identified, and dispersion of GNP. Copper salt was used to graft nano copper oxide particles and this technique was also tested for grafting other metal oxides such as iron oxide and was successfully tested. The grafting process and feedstock preparation are shown in Figures 38 and 39, respectively.

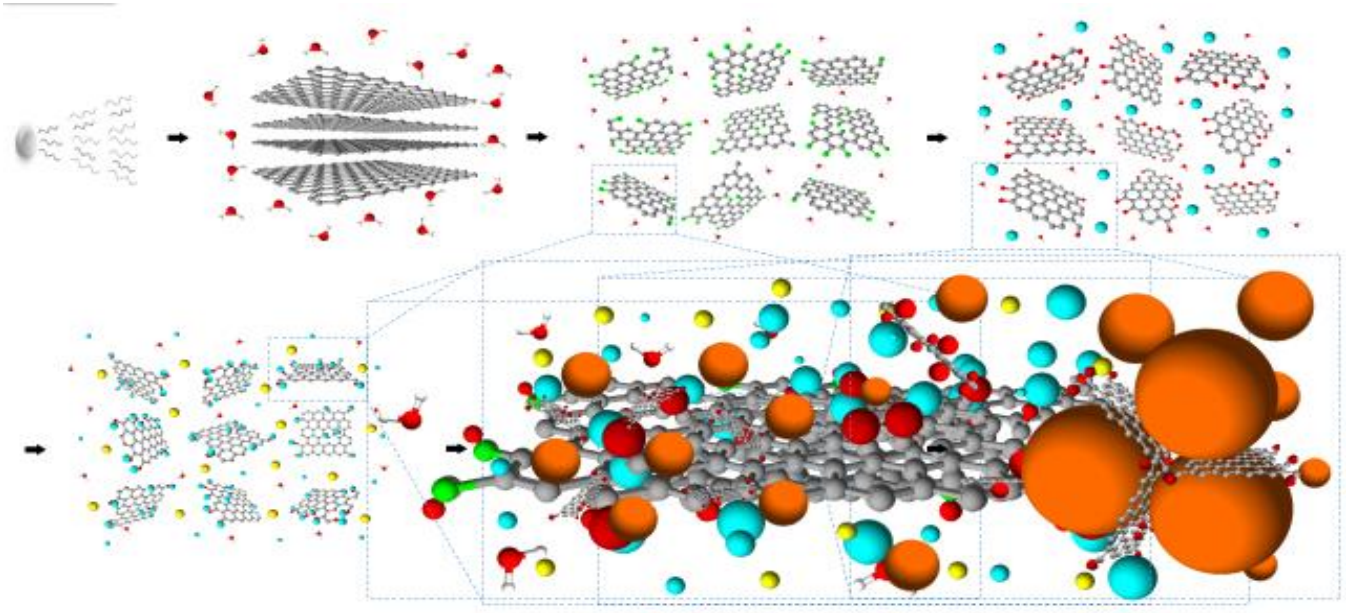

Figure 38: Methodology for graphene grafting.

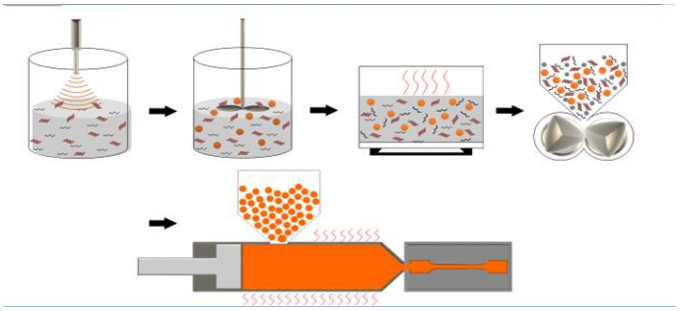

Figure 39: Feedstock preparation

The digital images of green injection molded parts are shown in Figure 40.

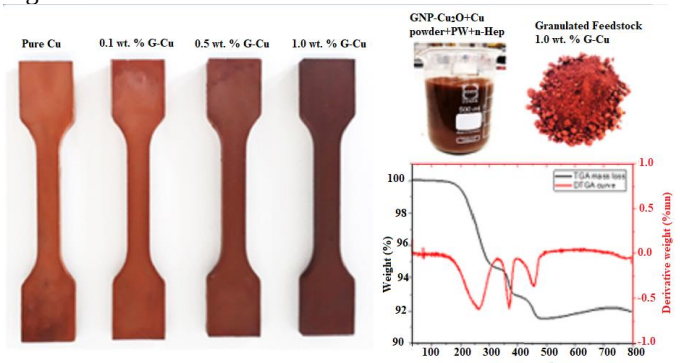

Figure 40: Powder injection molding

Development of High-Performance Fe-50Ni Soft Magnetic Alloy via Powder Injection Molding

The Fe-50Ni soft magnetic alloy was produced by powder injection molding using fine particle-size iron and nickel powders. The optimum loading was determined by measuring the critical loading and rheology of the feedstocks. The defect-free green parts were produced, and the binder was removed in two stages. The effect of processing parameters on densification, microstructure, and magnetic properties was investigated. The results confirmed that density and microstructure are closely associated with magnetic properties. The densification was enhanced, and grain size was improved with sintering temperature and time. The density of 98.02 % with a grain size of 240 microns was achieved at a sintering temperature of 1375ºC for a dwell time of 14 h under controlled cooling. The maximum magnetic permeability of 50240 and saturation induction of 1.52 Tesla was achieved.

Introduction

The Fe-50Ni soft magnetic alloys are used in various applications such as printers, relays, disk drive parts, and sensors. The development of the electronic industry requires micro size, multifunction, and intricate shape components for magnetic devices[93, 94]. The near-net-shape parts with micro-complex geometries can be produced by the traditional powder metallurgy process. However, the press-sinter technique is not suitable due to the presence of high porosity (about 10%) and poor microstructure in the final parts which result in lower magnetic properties. The Fe-50Ni alloy produced by casting and machining has maximum permeability of 70,000 and saturation induction of 1.6 Tesla [95]. The magnetic performance is excellent but the mass production of mini parts with complex geometry is highly limited due to low efficiency, long production run, and high cost [95, 96].

Powder injection molding is an advanced promising technology that combines the good attributes of powder metallurgy and plastic injection molding processes [97, 98]. The magnetic performance of Fe-50Ni alloys is strongly dependent on higher densification and large grain size. Many researchers have studied Fe-50Ni soft magnetic alloys by powder injection molding. Carreno et. al. [99] have reported a maximum permeability of 10,000 and magnetic induction of 1.4 Tesla. Miura et. al. [100] have reported the permeability and induction values as 27,000 and 1.37 T, respectively. Leonard et. al. [101] achieved the permeability and saturation induction as 20,000 and 1.37 respectively. Duan et al. [102] obtained a permeability of 33,830 and induction of 1.52 Tesla respectively. Jidong et. al. reported a maximum permeability of 43,541 and saturation induction of 1.48 Tesla[95]. There is limited work on the relationship between microstructure, density, and magnetic properties so far. This study provides a systematic study on the correlation between the microstructural and magnetic performance of Fe-50Ni soft magnetic alloy produced by PIM. Further, the cooling rate after sintering the injected parts plays an important role to control the grain size. The effect of controlled cooling on microstructure and associated properties is not investigated so far.

Materials and Methods

The high purity and fine particle size iron and nickel metallic powders were used in this study. Iron powder of 99.5 % and nickel powder of 99.1 % purity were used. The multi-component binder system used in this study consists of polypropylene (PP), paraffin wax (PW), and stearic acid (SA). The iron and nickel powders were mixed homogeneously in Turbular mixer for 6 h at 40 rpm. The critical powder volume percentage of 60.49 % was determined using a Brabender mixer. After that, three formulations of 60%, 58%, and 56% sloid loading were prepared for the rheology of the feedstocks. The binder consisted of 25% PP, 70% PW, and 5% SA. The formulation of 58% loading was selected as optimum loading and defect-free green parts were produced successfully by injection molding. Binder extraction is an important process to remove the main and supporting binder ingredients. The polymeric binder was removed in two phases namely solvent and thermal debinding. The solvent extraction was done by immersing green samples in n-heptane (C_7H_{16}) solution at 60˚C in a circulating water bath with an immersion time of 10 h. In thermal debinding, samples were heated at 600˚C for 120 minutes with a heating rate of 2˚C/min up to 400˚C and then 1˚C/min up to 600˚C as shown in Figure 41. The brown parts were sintered in a controlled reducing atmosphere at 1300ºC, 1325ºC, 1350 ºC, 1375ºC, and 1400ºC for 120 minutes with a heating and cooling rate. Then the temperature of 1375 ºC was selected for prolong sintering time because partial melting occurred at 1400ºC. The samples were sintered from 2 to 14 h with an increment of 2 h to enhance the densification. To investigate the effect of cooling rate on microstructure, the samples were cooled after sintering under a controlled cooling rate. The samples sintered at 1375ºC for 14 h and were cooled

at a cooling rate of 0.5ºC/min from 1375ºC to 1250ºC. The samples were held at 1350ºC, 1300ºC, and 1250ºC for a dwell time of 60 minutes during controlled cooling as shown in Figure 42. The sintered samples were characterized for physical, mechanical, microstructural, and magnetic properties. The densification of the sintered parts was measured by the Archimedes method and micro hardness was determined by the Vickers hardness tester. XRD was used to analyze the phase characteristics of the sintered samples and the microstructure was studied by optical microscopy and scanning electron microscopy. The magnetic performance was evaluated by using the MATS-2010-SD soft magnetic hysteresis curve tracer.

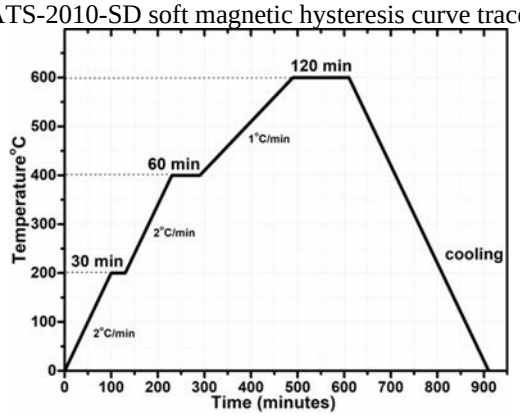

Figure 41: Thermal debinding curve of Fe-50Ni soft magnetic alloy

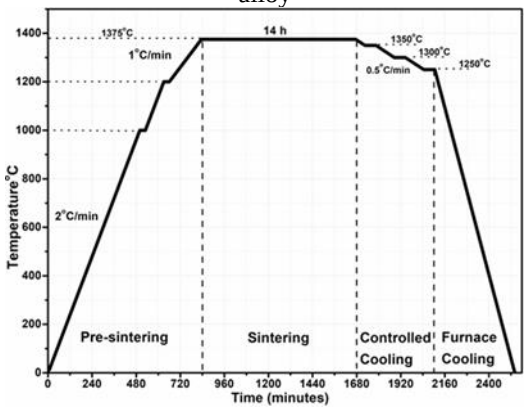

Figure 42: Sintering cycle of Fe-50Ni soft magnetic alloy with control cooling

Results and Discussion

The FESEM analysis of atomized powders revealed that iron particles were rounded in shape without any agglomeration. According to particle size analysis, the average particle size of the iron was 3.0 µm and with 99.5 % purity. Whereas nickel particles were regular in shape without any agglomeration and have an average particle size of 2.1 µm with 99.1% purity. In this study, the critical loading of the Fe and Ni mixed powders was determined 60.49% and feedstock with powder loading of 58 vol% was optimized by rheology. The feedstock with optimized loading was successfully injection molded and the injected green parts were free from physical defects. The feedstock was analyzed by FESEM for homogeneity of the binder and powders, and it was found homogeneous due to voids filling by the binder between the metal particles as shown in Figure 43. The binder was removed in two stages. In the first stage of debinding, the binder diffuses to the solvent from the green parts due to capillary forces and produces very fine pore channels that facilitate the removal of the remaining backbone binder through thermal debinding. Solvent temperature is the key factor that affected the diffusivity and solubility of the binders in an n-heptane solution. Therefore, the melting points of the binders were measured by DSC analysis to determine the solvent debinding temperature. The melting temperature of the PW is 58ºC therefore solvent extraction was done at a temperature of 60ºC for 10 h. In the second stage, thermal debinding was carried out to remove the backbone polymer. The heating cycle for the thermal removal of PP was designed based on TGA results. The SA and PW decomposition started at 190ºC-230ºC and was eliminated at about 300ºC-400ºC temperature range. The backbone polymer PP degradation started after 330ºC and completely decomposed at about 500ºC. The multi-component binders decomposed gradually in a wide temperature range starting from 190ºC to 500ºC approximately. The wide-ranging gradual decomposition produces a network of porous channels which facilitate the outflow of decomposition gases during thermal debinding. In the first step at 200°C, the dwell time of 30 min was given for homogenization of the temperature. The PW and SA decomposed at 400°C, therefore dwell time of 60 minutes was given for their complete elimination and for the formation of porous channels to remove the PP.

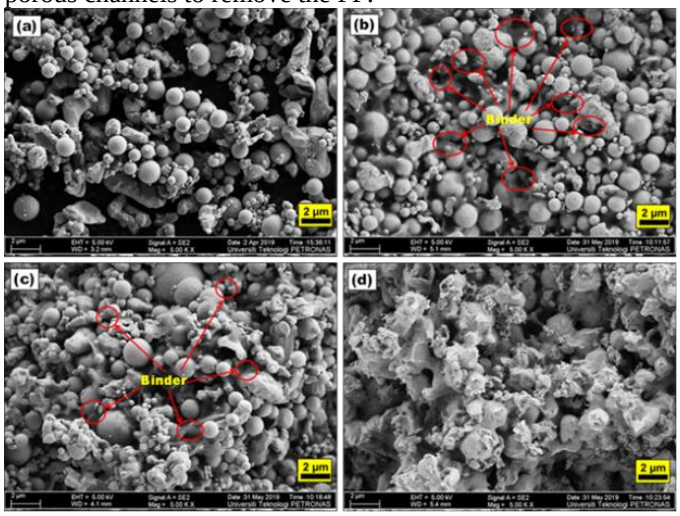

Figure 43: FESEM images of (a) Fe and Ni mixed powder (b) Feedstock with 58 vol% powder loading (c) green part after solvent debinding (d) brown part after thermal debinding.

The sintering temperature has a significant effect on densification. There was significant porosity at grain boundaries and within the grains at 1300ºC and 1325ºC sintering temperatures. The grain growth was retarded due to the presence of porosity and average grain size of 30-40 microns was achieved at 1325ºC as shown in Figure 44. The porosity has been reduced with the increase in sintering temperature resulting in higher densification. The average grain size increased to 90 µm at 1375ºC.

Most of the porosity shifted towards the grain boundaries and triple points and a lesser amount is entrapped within the grains. The samples were partially melted at 1400ºC; therefore, the sintering time was enhanced to 14 h. The density was increased up to 12 h of sintering and after that it became constant. The

densification was enhanced to 98.02% and grain size was improved to 220 microns. Then, the controlled cooling rate was employed, and grain size was improved to 240 microns as shown in Figure 45. Vickers hardness of sintered specimens was measured, and it was observed that hardness increased with the increase in densification. The maximum hardness was achieved at 138 HV at densification of 98 %.

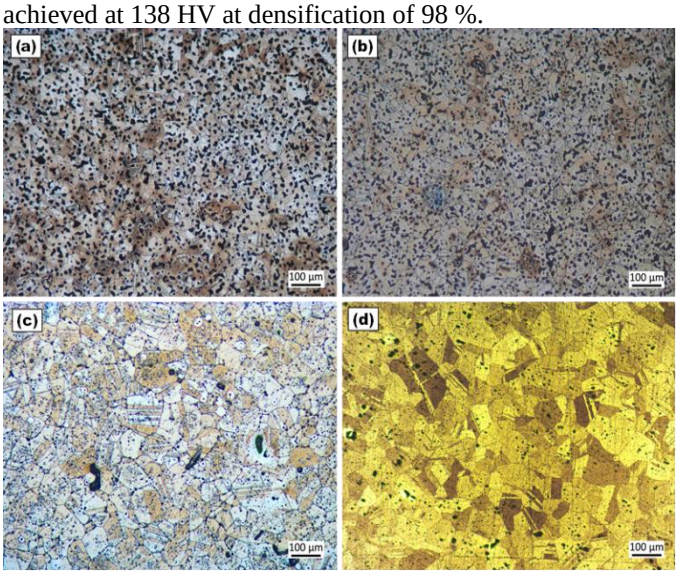

Figure 44: Microstructure of Fe-50Ni alloy sintered at (a) 1300ºC, (b) 1325ºC, (c) 1350ºC, (d) 1375ºC

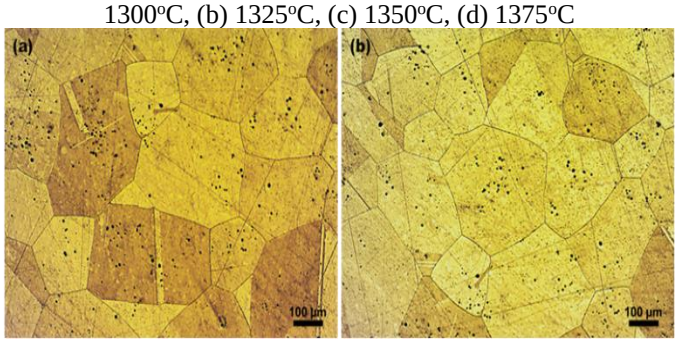

Figure 45: Optical micrographs of Fe-50Ni soft magnetic alloy sintered at 1375ºC and cooled with a controlled cooling rate

X-ray diffraction pattern of Fe-Ni blended powders before feedstock preparation is shown in Figure 46 (a). The XRD data were analyzed by using HighScore Plus software available in UTP central analytical laboratory facilities. Iron peaks of planes (110), (002), and (121) were detected (Iron ICSD:64999, PANICSD:98-006-4999) while nickel peaks of planes (111), (200), and (220) were detected (Nickel ICSD:163354, PANICSD:98-016-3354) as main phases in the Fe-Ni mixture powder. After sintering, Fe and Ni peaks disappeared and only peaks of the γ-FeNi phase were detected (Austenite ICSD:186833, PANICSD:98-018-6833) which indicates the complete alloy formation. All the peaks of planes (111), (200), (220), (113), and (222) of the austenite FCC phase were detected as can be clearly seen in Figure 46. The magnetic permeability was improved to 50240 which is more than the previous maximum reported value of 43,541. The hysteresis curve is shown in Figure 47. High magnetic performance electromagnetic components can be produced with reduced volume. Hence, size reduction would save cost and fulfil the current industrial requirements of miniaturization. A brief comparison of the reported and achieved physical and magnetic properties of Fe-50Ni soft magnetic alloy is provided in Table 10.

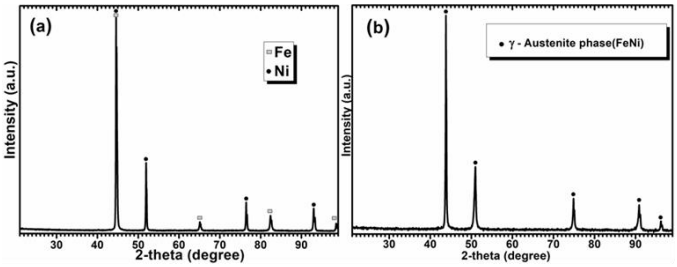

Figure 46: XRD pattern of (a) Fe and Ni mixed powder (b) sintered sample

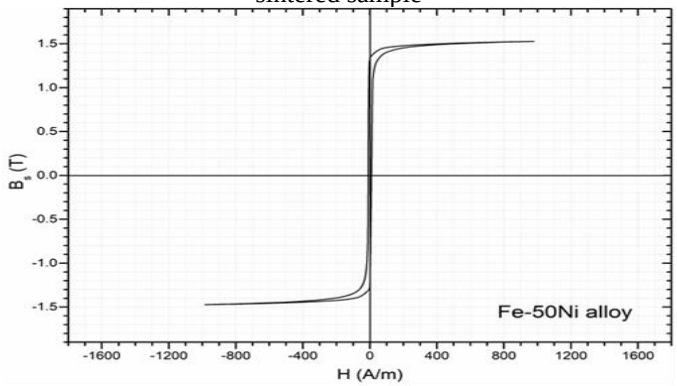

Figure 47: Hysteresis loop of Fe-50Ni soft magnetic alloy by powder injection molding.

Both higher sintering temperature and sintering time have combined effects on grain size and magnetic permeability. Bigger grain size is allowing more magnetic flux however the magnetic field strength is declining. This project is still running, and intense characterization will be made to find out different aspects.

Development of 316L SS Medical implant in Addition to Nano-Titanium Powders for Improved Physical and Mechanical Properties.

Introduction

With the advancement of medical science, the life expectancy of humans has been increasing significantly, and geriatric diseases like orthodontics and bone diseases have been increasing gradually. Very often bone needs to be replaced by biomedical parts. Material selection is vital for biomedical parts since most of the materials are not so bio-compatible and has adverse effects on the human body in the long run [103]. Additionally, when the orthopedic implant is concerned the implanted part should have an almost similar modulus to the actual bone (10-30 GPa) [104]. If the implant-bone has a much higher modulus mean it will carry the maximum load and results in a stress-shielding effect on the other bone. Therefore, maintaining the low Young's modulus is challenging. Moreover, as the body parts are experiencing a continuous dynamic loading surrounded by the hostile body fluid condition, the creep resistance property is also vital for the implanted materials [105]. Hybrid 316L SS alloy with metallic bio-inert material like nano-titanium powder may enhance the

mechanical properties and shall be more compatible with living human tissue. Titanium is considered biocompatible material for permanent implants and Ti components can be found in neurosurgery (Nonpenetrating titanium anastomotic clips) [106, 107], Artificial eye implants (especially in titanium sleeve and peg and Ti orbital) [108], spinal fusion cages [109], pacemakers, hearing aid device [110] and dental screw, bone implant, joint replacement [103, 111]. Moreover, varying material volume, particle shape, and size, injection temperature, debinding, sintering parameters, etc. have been accustomed to improving the implant quality and biocompatibility.

Feedstock preparation

In this research work, one of the objectives is to compare the improvement of biocompatibility for the addition of Ti Nano powders. Therefore, three feedstocks were prepared for sample preparation varying Ti powders vol%. In Table 11. the feedstock compositions are given below.

Table 11: different compositions of feedstocks

	316L SS	Nano Ti	Binders
Feedstock 1	64%	1%	35%
Feedstock 2	62%	3%	35%
Feedstock 3	60%	5%	35%

Using these feedstocks dogbone samples are prepared and the effects of adding nano Ti will be observed in mechanical strength and corrosion behavior in simulated body fluid. This research is also an ongoing project.

Development of Metal Parts Using Additive Manufacturing

These days, Additive Manufacturing (AM) or 3D printing has become a viable option for manufacturers for fabricating metals, plastics, ceramics, and composites as this technology does not need any specific mold requirement. AM includes Stereolithography, Selective Laser Melting (SLM), Electron Beam Melting (EBM), Binder Jetting (BJ), Direct Energy Deposition (DED), and Fused Deposition Modelling (FDM) process [112]. Every process has its pros and cons. In terms of a cost-effective approach, FDM is the most attractive technology option for manufacturers. In FDM, first, we need to design part shapes in AutoCAD [112]. This CAD file is sliced and fed into 3D Printer. After giving the file to 3D Printer, the filament which consists of a thermoplastic binder along with metal particles is extruded around 200C over the printing bed as per sliced CAD file instructions. In this way, the green part is made, and this green part is gone through subsequent de-binding and sintering processes for making a densified and fully metallic part. Although the metal part made through FDM is an economical method, the mechanical properties of the final metal part are weak in comparison to other processes. In this regard, varying Printing, and Subsequent process parameters are to be performed for enhancing the mechanical strength of Ultrafuse BASF 316L SS parts made through FDM.

Future Trends and Opportunities

Although powder metallurgy (PM) is facing challenges in finding a new arena of applications, the enormous flexibility of using materials, properties, processing, mass production with complex geometry make this technique a sustainable method of fabrication parts. Additive manufacturing, an emerging technique, is also a powder-based fabrication method drawing attention recently; however, this technique is yet to replace the conventional PM by far [113]. Soft magnets, extremely hard Neodymium magnets, refractory materials, fast-growing medical arena, i.e., degradable, and nondegradable bio-compatible medical implant, Implant drug delivery system, introduction of nano properties in macro-objects, etc. can be done easily and controllably by using PM. Moreover, smart alloys and functional materials can be made by using PM.

Table 10: Comparison of the previous and present research

Author	Composition	Sintering Parameter		Density %	Grain Size µm	Magnetic properties		
		t(h)	T (°C)			μ_m	B_s tesla	H_c A/m
Carreno et. al. [99]	Fe-50Ni	2	1300	95.8	32-45	10000	1.4	-
Miura et. al. [100]	Fe-50Ni	1	1350	95-96	-	19500	1.56	15.9
Leonardo et. al. [101]	Fe-47Ni	50	1260	92.4	-	20000	1.29	20
		3	1330	96.5	-	20000	1.37	21
Bohua et. al. [102]	Fe-50Ni	2	1380	97	70-90	33810	1.52	16.6
Jidong et. al. [95]	Fe-50Ni	10	1360	97	100-200	43541	1.48	6.8
Present invention	Fe-50Ni	14	1375	98.02	220-240	50240	1.52	9.9

Conclusion

To recapitulate, the AFM group of UTP is among the pioneers in the PIM sector in Malaysia. This technique has been utilized successfully for several industrial applications and research accomplished has provided important findings. An improved corrosion rate of 0.12 mpy has been achieved using a 10 °C/min cooling rate for sintered 316L and a negligible amount of metal ions release of 0.0001 ppm has been recorded for 316L sintered SS. In the case of modified 316L SS with boron and titanium powder for dental screws, highly dense final parts have been achieved with less cytotoxicity. Some noble works i.e., carbon nanotubes reinforced Cu-matrix nanocomposites achieved a significant improvement in thermal conductivity, hardness, and Young's modulus. Grafting metallic oxide on graphene nanoplatelets is one of the most remarkable achievements. Moreover, creating a soft magnet by using PIM with improved magnetic permeability of 50240 has surpassed all the previous findings in PIM of soft magnets. The ongoing projects on PIM are expected to achieve the desired objectives as well.

Acknowledgment

I would like to thank contributing authors and university Teknologi PETRONAS, Perak Malaysia for financial and laboratory support. We are thankful, MOSTI, Government of Malaysia for providing Techno-Fund for the pre-commercialization of nano copper composites for the thermal management of LED light.

References

1. Noorsyakirah, A., et al., *Application of potassium carbonate as space holder for metal injection molding process of open pore copper foam.* 2016. **19**: p. 552-557.
2. Abolhasani, H. and N.J.J.o.m.p.T. Muhamad, *A new starch-based binder for metal injection molding.* 2010. **210**(6-7): p. 961-968.
3. Raza, M.R., et al., *Effects of cooling rate on mechanical properties and corrosion resistance of vacuum sintered powder injection molded 316L stainless steel.* 2012. **212**(1): p. 164-170.
4. Jamaludin, M.I., *Development of porous TI-6AL-4V mix with palm stearin binder by metal injection moulding technique*. 2015, Universiti Teknologi Mara.
5. Aslam, M., et al., *Low pressure injection molding of boron admixed 316l stainless steel for engineering applications.* 2006.
6. Aslam, M., et al. *Effects of admixed titanium on densification of 316L stainless steel powder during sintering*. in *MATEC Web of Conferences*. 2014. EDP Sciences.
7. Naseer, A., et al., *A review of processing techniques for graphene-reinforced metal matrix composites.* 2019. **34**(9): p. 957-985.
8. Muhsan, A.S. and F. Ahmad. *Development of nanocomposites heat sink (MWCNTs/Cu) using powder injection moulding for electronic applications*. in *2011 National Postgraduate Conference*. 2011. IEEE.
9. Ali, M., F.J.M. Ahmad, and M. Processes, *A review of processing techniques for Fe-Ni soft magnetic materials.* 2019. **34**(14): p. 1580-1604.
10. Aleksandra Kocijan and Marjetka Conradi, *The corrosion behaviour of austenitic and duplex stainless steels in artificial body fluids.* Materials and technology, 2010. **44**(1): p. 21-24.
11. Geetha Manivasagam, Durgalakshmi Dhinasekaran, and Asokamani Rajamanickam, *Biomedical Implants: Corrosion and its prevention - A Review.* Recent Patents on Corrosion Science, 2010. **2**: p. 40-54.
12. Anil Kurella and Narendra B. Dahotre, *Review paper : Surface modification for bioimplants : The role of laser surface.* Journal of Biomaterials Applications, 2005. **20**: p. 5-50.
13. Balamurugan A., Kannan S., and Rajeswari S., *Structural and electrochemical behaviour of sol-gel zirconia films on 316L stainless-steel in simulated body fluid environment.* Materials Letters, 2003. **57**: p. 4202-4205.
14. Abenojar J, et al., *Reinforcing 316L stainless steel with intermetallic and carbide particles.* Materials Science and Engineering A, 2002. **335**: p. 1-5.
15. Tang J, et al., *The preparation of corrosion resistant palladium films on 316L stainless steel by brush plating.* Surface and Coatings Technology, 2010. **204**(9-10): p. 1637-1645.
16. García C., et al., *Pitting corrosion behaviour of PM austenitic stainless steels sintered in nitrogen – hydrogen atmosphere.* Corrosion Science, 2007. **49**: p. 1718-1736.
17. Esmaeil Jafari and Mohammad Jafar Hadianfard, *Influence of surface treatment on the corrosion resistance of stainless steel in simulated human body environment.* 2009. **25**(5): p. 611-614.
18. Baron A., et al., *Influence of electrolytic polishing on electrochemical behaviour of austenitic steel.* Journal of Achievements in Materials and Manufacturing Engineering, 2006. **18**(1-2): p. 55-58.
19. Kargar B.S., et al., *Improving the corrosion behaviour of powder metallurgical 316L alloy by prepassivation in 20% nitric acid.* Corrosion Science, 2010.
20. Zaid Bou-Saleh, Abdullah Shahryari, and Sasha Omanovic, *Enhancement of corrosion resistance of a biomedical grade 316LVM stainless steel by potentiodynamic cyclic polarization.* Thin Solid Films, 2007. **515**(11): p. 4727-4737.
21. Chun-Che Shih, et al., *Effect of surface oxide properties on corrosion resistance of 316L stainless steel for biomedical applications.* Corrosion Science, 2004. **46**: p. 427-441.
22. Tiwari S.K., et al., *Development and characterization of sol–gel silica–alumina composite coatings on AISI 316L for implant applications.* Surface & Coatings Technology, 2007. **201**: p. 7582-7588.

23. Peyre P., et al., *Surface modifications induced in 316L steel by laser peening and shot-peening . Influence on pitting corrosion resistance.* Materials Science and Engineering A, 2000. **280**: p. 294-302.
24. Mohammad Hossein Fathi and Vajihesadat Mortazavi *Tantalum, Niobium and Titanium coatings for biocompatibility improvement of dental implants.* Dental Research Journal, 2007. **4**(2): p. 74-82.
25. Gopi, D., et al., *Evaluation of hydroxyapatite coatings on borate passivated 316L SS in Ringer's solution.* 2009. **29**(3): p. 955-958.
26. Disegi J A and Eschbach L, *Stainless steel in bone surgery* Injury, Int. J. Care Injured 2000. **31**: p. S-D2-6.
27. Dean-Mo Liu, Quanzu Yang, and Tom Troczynski, *Sol–gel hydroxyapatite coatings on stainless steel substrates.* Biomaterials, 2002. **23**: p. 691-698.
28. Kannan S, Balamurugan A, and Rajeswari S, *Electrochemical characterization of hydroxyapatite coatings on HNO_3 passivated 316L SS for implant applications.* Electrochimica Acta, 2005. **50**: p. 2065-2072.
29. Essa, K., et al., *Porosity control in 316L stainless steel using cold and hot isostatic pressing.* Materials & Design, 2018. **138**: p. 21-29.
30. Beebhas C, Mutsuddy, and Renée G. Ford, *Ceramic injection molding*. 1995, Chapman & Hall, London, UK.
31. German R M and B. A, *Powder injection molding of metal and ceramics*. 1997: Metal Powder Industries Federation, Princeton, N.J.
32. Reinshagen J H and Neupaver A J, *Fundamentals of P/M stainless steels.* Advances in Powder Metallurgy., 1989. **2**: p. 283-295.
33. Research, G.V. *Metal Injection Molding (MIM) Market Analysis By End-Use (Automotive, Consumer Product, Medical, Industrial, Defense), By Region (North America, Europe, Asia Pacific, CSA, MEA),Competitive Landscape, And Segment Forecasts, 2018 - 2025*. 2016 [cited 2019 09-08-2019]; Available from: https://www.grandviewresearch.com/industry-analysis/metal-injection-molding-mim-market.
34. Barriere T, Gelin J C, and Liu B, *Experimental and numerical investigations on properties and quality of parts produced by MIM.* Powder Metallurgy, 2001. **44**(3): p. 228-234.
35. Quinard C, T. Barriere, and C. Gelin, *Development and property identification of 316L stainless steel feedstock for PIM and µPIM.* powder technology, 2009. **190**: p. 123-128.
36. Zlatkov B S, et al., *Recent advances in PIM technology I.* Science of Sintering, 2008. **40**: p. 79-88.
37. Stephenson, D.J.A.a.P.D., *The Powder Injection Moulding Process*. 2001.
38. Tassin, C., et al., *Carbide-reinforced coatings on AISI 316 L stainless steel by laser surface alloying.* Surface and Coatings Technology, 1995. **76-77, Part 2**(0): p. 450-455.
39. Ruangdaj Tongsri, et al., *Effect of powder mixture conditions on mechanical properties of sintered Al_2O_3-SS 316L composites under vacuum atmosphere.* Journal of Metals, Materials and Minerals., 2007. **17**(1): p. 81-85.
40. Ibrahim M H I, et al. *Water atomised stainless steel powder for micro metal injection molding: Optimization of rheological properties*. in *Malaysian Metallurgical Conference-MMC2008*. 2008. UKM, Bangi, Malaysia
41. Yimin Li, et al., *Thermal debinding processing of 316L stainless steel powder injection molding compacts.* Journal of Materials Processing Technology, 2003. **137**: p. 65-69.
42. Jamaludin Khairur Rijal, et al. *Temperature influence to the injection molding of fine and coarse SS316L powder with PEG, PMMA and stearic acid binder system*. in *Proceeding of Malaysian Symposium on Advances in Powder Metallurgy & Particulate Materials*. 2007. Faculty of Mechanical Engineering, University Technology MARA.
43. Yoshistato Kiyota, *Starting material for injection molding of metal powder and method of producing sintered parts*, US, Editor. 1989: Japan.
44. Ji C. H. , et al., *Sintering study of 316L stainless steel metal injection molding parts using Taguchi method: Final density.* Materials Science and Engineering, Vol. A311, 2001. **311**: p. 74-82.
45. Jamaludin K.R., et al. *Sintering parameter optimization of the SS316L metal injection molding (MIM) compacts for final density using taguchi method*. in *3rd South East Asian Technical University Consortium,*. 2009. Johor Bahru, Malaysia.
46. Manam, N.S., et al., *Sintering temperature effects on the properties of stainless steel 316L compact fabricated by metal injection moulding.* International Journal of Manufacturing Technology and Management, 2019. **33**(1-2): p. 37-52.
47. Martin, F., C. Garcia, and Y. Blanco, *Effect of chemical composition and sintering conditions on the mechanical properties of sintered duplex stainless steels.* Materials Science and Engineering: A, 2011. **528**(29-30): p. 8500-8511.
48. Raza, M.R., et al., *Effects of solid loading and cooling rate on the mechanical properties and corrosion behavior of powder injection molded 316 L stainless steel.* Powder technology, 2016. **289**: p. 135-142.
49. Raza, M.R., et al., *Effects of debinding and sintering atmosphere on properties and corrosion resistance of powder injection molded 316L-stainless steel.* Sains Malaysiana, 2017. **46**(2): p. 285-293.
50. Ruangdaj Tongsri, S.A., Chanchai Mateepithukdharm, Thummasin Piyarattanatrai, and W. Panyawat, *Effect of powder mixture conditions on mechanical properties of sintered Al2O3-SS 316L*

composites under vacuum atmosphere. Journal of Metals, Materials and Minerals, 2007. **17**: p. 81-85.
51. Suharno, B., et al. *Effect of powder loading on local feedstock injection behavior for fabrication process of orthodontic bracket SS 17-4 PH using metal injection molding*. in *AIP Conference Proceedings*. 2019. AIP Publishing.
52. Supriadi, S., et al. *Preparation of feedstock using beeswax binder and SS 17-4PH powder for fabrication process of orthodontic bracket by metal injection molding*. in *AIP Conference Proceedings*. 2019. AIP Publishing.
53. C.H. Ji, et al., *Sintering study of 316L stainless steel metal injection molding parts using Taguchi method: Final density*. Materials Science and Engineering, 2001. **311**: p. 74-82.
54. Andrew Coleman, et al., *Effects of powder size and chemistry on densification and properties of 316L MIM parts made under different sintering atmospheres.* PIM International, 2013. **7**(2): p. 6.
55. Muhammad Rafi Raza, et al., *Development of Defects Free Stainless Steel Parts Using Powder Injection Molding.* Asian Journal of Scientific Research, 2013. **6**: p. 307-314.
56. F. Martín, C. García, and Y. Blanco, *Effect of chemical composition and sintering conditions on the mechanical properties of sintered duplex stainless steels.* Materials Science and Engineering: A, 2011. **528**(29): p. 8500-8511.
57. Khairur R.Jamaludin, et al., *Optimizing the injection parameter of water atomised SS316L powder with design of experiment method for best sintered density.* Chiang Mai J. Sci., 2009. **36**(3): p. 349-358.
58. Nattaya Tosangthum, et al., *Density and strength improvement of sintered 316L stainless steel.* Chiang Mai J. Sci., 2006. **33**(1): p. 53-66.
59. Raza, M.R., et al., *Effects of cooling rate on mechanical properties and corrosion resistance of vacuum sintered powder injection molded 316L stainless steel.* Journal of Materials Processing Technology, 2012. **212**(1): p. 164-170.
60. R.M. German and A. Bose, *Powder injection molding of metal and ceramics*. 1997: Metal Powder Industries Federation, Princeton, N.J.
61. Animesh Bose, et al., *Faster sintering and lower costs with ultra-fine MIM powders.* Metal Powder Report, 2008(May): p. 25-30.
62. B. S. Becker, J. D. Boltom, and A. M Eagles. *Sintering of 316L stainless steels to high density via the addition of chromium-molybdenum dibromide powders Part1: Sintering performance and mechanical properties*. in *Proceedings of the Institution of Mechanical Engineers. Part L, Journal of materials, design and applications*. 2000. LHL.
63. Zhang, Y., et al., *On the Microstructures and Fatigue Behaviors of 316L Stainless Steel Metal Injection Molded with Gas- and Water-Atomized Powders.* 2018. **8**(11): p. 893.
64. Davis, J.R., *Stainless steels*. 1994: ASM international.
65. Allen J. Bard, Martin Stratmann, and Gerald S. Frankel, eds. *Encyclopedia of electrochemistry: Corrosion and oxide films*. Vol. 4. 2003, WILEY-VCH.
66. Steffen Krug and Stefan Zachmann, *Influence of sintering conditions and furnace technology on chemical and mechanical properties of injection molded 316L.* Powder Injection Moulding International, 2009. **3**(4): p. 66-70.
67. Črtomir Donik, et al., *XPS study of duplex stainless steel oxidized by oxygen atoms.* Corrosion Science, 2009. **51**(4): p. 827-832.
68. Muterlle P.V., Perina M., and Molinari A., *Mechanical properties and corrosion resistance of vacuum sintered MIM 316L stainless steel containing delta ferrite.* PIM International, 2010. **4**(2): p. 66-70.
69. Johnson J.L., et al., *Mechanical properties and corrosion resistance of MIM Ni-based superalloys.* 2004.
70. Jeffrey A. Platt, et al., *Corrosion behavior of 2205 duplex stainless steel.* American Journal of Orthodontics and Dentofacial Orthopedics, 1997. **112**(1): p. 69-79.
71. Gopi D., et al., *Evaluation of hydroxyapatite coatings on borate passivated 316L SS in Ringer 's solution.* Materials Science & Engineering C, 2009. **29**: p. 955-958.
72. Christine Trepanier, Ramakrishna Venugopalan, and Alan R. Pelton, *Corrosion resistance and biocompatibility of passivated Nitinol*. 2000. p. 35-45.
73. Christine Trepanier and Alan R.Pelton, *Biocompatibality and corrosion resistance of NiTi*. Cordis-NDC: CA.
74. Witte F., et al., *Degradable biomaterials based on magnesium corrosion.* Current Opinion in Solid State and Materials Science, 2008. **12**(5-6): p. 63-72.
75. Fariborz Amini, et al., *Metal ion release from fixed orthodontic appliances — an in vivo study.* The European Journal of Orthodontics, 2011(1997): p. 1-5.
76. Macedo De Menezes L. and Cardoso Abdo Quintão C., *The release of ions from metallic orthodontic appliances.* Seminars in Orthodontics, 2010. **16**(4): p. 282-292.
77. Singh Raghuvir and Dahotre Narendra B. , *Corrosion degradation and prevention by surface modification of biometallic materials.* J Mater Sci: Mater Med, 2007. **8**: p. 725-751.
78. Heaney, D., *Handbook of metal injection molding*. 2012: Elsevier.
79. Meng, J., et al., *Replication and characterization of 316L stainless steel micro-mixer by micro powder injection molding.* Journal of Alloys and Compounds, 2010. **496**(1): p. 293-299.

80. Ferreira, T., et al., *Mechanical behaviour of dental implants manufactured from metallic powders by μMIM.* Ciência & Tecnologia dos Materiais, 2014. **26**(2): p. 89-95.
81. Ismail, M.H., et al., *FEEDSTOCK FLOW CHARACTERIZATION AND PROCESSING OF POROUS NITI BY METAL INJECTION MOULDING (MIM).* Jurnal Teknologi, 2015. **76**(11).
82. Rajabi, J., et al., *Fabrication of miniature parts using nano-sized powders and an environmentally friendly binder through micro powder injection molding.* Microsystem Technologies, 2015. **21**(5): p. 1131-1136.
83. Wang, Q., et al., *Single iridium atom doped Ni2P catalyst for optimal oxygen evolution.* 2021. **143**(34): p. 13605-13615.
84. Nan, C.-W., Z. Shi, and Y. Lin, *A simple model for thermal conductivity of carbon nanotube-based composites.* Chemical Physics Letters, 2003. **375**(5-6): p. 666-669.
85. Nan, C.-W., et al., *Interface effect on thermal conductivity of carbon nanotube composites.* Applied Physics Letters, 2004. **85**(16): p. 3549-3551.
86. Cho, S., et al., *Multiwalled carbon nanotubes as a contributing reinforcement phase for the improvement of thermal conductivity in copper matrix composites.* Scripta Materialia, 2010. **63**(4): p. 375-378.
87. Chu, K., et al., *Fabrication and effective thermal conductivity of multi-walled carbon nanotubes reinforced Cu matrix composites for heat sink applications.* Composites Science and Technology, 2010. **70**(2): p. 298-304.
88. Kim, K.T., et al., *Influence of embedded-carbon nanotubes on the thermal properties of copper matrix nanocomposites processed by molecular-level mixing.* Scripta Materialia, 2011. **64**(2): p. 181-184.
89. Twinkle, C. and J.J.A.M.M. Pitchaimani, *A semi-analytical nonlocal elasticity model for static stability and vibration behaviour of agglomerated CNTs reinforced nano cylindrical panel under non-uniform edge loads.* 2022. **103**: p. 68-90.
90. Agarwal, A., S.R. Bakshi, and D. Lahiri, *Carbon nanotubes: reinforced metal matrix composites*. 2018: CRC press.
91. Tjong, S.C., *Carbon nanotube reinforced composites.* NY: Wiley-VCH, 2009.
92. Cha, S.I., et al., *Extraordinary strengthening effect of carbon nanotubes in metal-matrix nanocomposites processed by molecular-level mixing.* Advanced Materials, 2005. **17**(11): p. 1377-1381.
93. German, R.M., *Injection molding of metals and ceramics.* Metal powder industries federation, 1997. **3**.
94. Aslam, M., et al., *Powder injection molding of biocompatible stainless steel biodevices.* Powder Technology, 2016. **295**: p. 84-95.
95. Ma, J., et al., *Microstructure and magnetic properties of Fe–50% Ni alloy fabricated by powder injection molding.* Journal of Magnetism and Magnetic Materials, 2013. **329**: p. 24-29.
96. Lall, C., *SOFT MAGNETISM Fundamentals for powder metallugy and Metal injection molding.* Monographs in P/M Series, 1992(2).
97. KULKARNI, K., *Metal Powders and feedstocks for metal injection molding.* Int. J. Powder Metall., 2000. **36**: p. 42-52.
98. Whittaker, D., *MIM soft magnetic materials: processing, properties and applications.* Powder Metallurgy Technology, 2016(4): p. 14.
99. Carreño-Morelli, E., et al., *Fe2. 7Si, Fe50Ni and Fe50Co Soft Ferromagnetic Materials by Powder Injection Moulding.*
100. Miura, H. and H. Kang, *Application of metal injection moulding to soft magnetic materials.* Powder Metallurgy, 2013. **56**(1): p. 38-45.
101. Lopes, L.U., et al. *Study of soft magnetic nickel-iron based alloys processed by powder injection molding*. in *Materials Science Forum*. 2008. Trans Tech Publ.
102. Bohua, D., et al., *Powder injection molding of Fe-Ni soft magnetic alloys.* Rare Metals, 2006. **25**(6): p. 440-444.
103. Hamidi, M., et al., *A review of biocompatible metal injection moulding process parameters for biomedical applications.* 2017. **78**: p. 1263-1276.
104. Ramsden, J.J., et al., *The design and manufacture of biomedical surfaces.* 2007. **56**(2): p. 687-711.
105. Saini, M., et al., *Implant biomaterials: A comprehensive review.* 2015. **3**(1): p. 52.
106. Mishinov, S., et al., *Titanium patient-specific implants in reconstructive neurosurgery.* 2018. **52**(3): p. 152-155.
107. Kaufman, B.A., et al., *Spinal dural closure with nonpenetrating titanium clips in pediatric neurosurgery.* 2010. **6**(4): p. 359-363.
108. Jordan, D.R., S.R.J.O.P. Klapper, and R. Surgery, *A new titanium peg system for hydroxyapatite orbital implants.* 2000. **16**(5): p. 380-387.
109. Fujibayashi, S., et al., *A novel synthetic material for spinal fusion: a prospective clinical trial of porous bioactive titanium metal for lumbar interbody fusion.* 2011. **20**(9): p. 1486-1495.
110. Horstink, L., et al., *Titanium fixtures for bone-conduction devices and the influence of type 2 diabetes mellitus.* 2012. **33**(6): p. 1013-1017.
111. Bansiddhi, A. and D. Dunand, *Titanium and NiTi foams for bone replacement*, in *Bone Substitute Biomaterials*. 2014, Elsevier. p. 142-179.
112. Prabhakar, M.M., et al., *A short review on 3D printing methods, process parameters and materials.* 2021. **45**: p. 6108-6114.
113. Danninger, H.J.P.M.P., *What will be the future of powder metallurgy?* 2018. **18**(2): p. 70-79.